Response to Referee #1

Comment 1

Pg 2, Line 51. "Another effect caused by the horizontally oriented columns is the corner reflection when the lidar is tilted at 30 deg..." The 30 deg corner reflection comes from plates, not columns. Columns also have a corner reflection but it is closer to 60degrees. This is noted in A. Borovoi, I. Grishin, E. Naats, and U. Oppel, "Backscattering peak of hexagonal ice columns and plates," Opt. Lett. 25(18), 1388–1390 (2000).

Response

Yes you are right. Depolarization of backscattered radiation has a maximum at a lidar tilt of 30 degrees for oriented plates and about 60 degrees for columns (Borovoi et al., 2000). A more detailed simulations show that when angular reflection is taken into account, the element a_{44} of the BSPM is most informative in determining of the flutter (Konoshonkin, 2016). For the plates, an abrupt change in the a_{44} occurs at a tilt angle of 30 degrees, while for the columns this element begins to grow smoothly at 30 degrees and reaches a maximum at 60° (Konoshonkin et al., 2016).

Reference to add:

Borovoi, A., Grishin, I., Naats, E., and Oppel, U., "Backscattering peak of hexagonal ice columns and plates," Opt. Lett., 25(18), 1388–1390 (2000).

Konoshonkin, A.V., "Simulation of the scanning lidar signals for a cloud of monodisperse quasi-horizontal oriented particle," Optika Atmosfery i Okeana, 29, No. 12, 1053–1060 (2016) [in Russian].)

Revised text

Another effect caused by the horizontally oriented plates and columns is the corner reflection. It appears when the lidar is tilted at a significant angle. Depolarization of backscattered radiation has a maximum at a lidar tilt of 30 degrees for oriented plates and about 60 degrees for columns (Borovoi et al., 2000). A more detailed simulations show that when angular reflection is taken into account, the element a_{44} of the light backscattering phase matrix (BSPM) is most informative in determining of the flutter (Konoshonkin, 2016). For the plates, an abrupt change in the a_{44} occurs at a tilt angle of 30 degrees, while for the columns this element begins to grow smoothly at 30 degrees and reaches a maximum at 60° (Konoshonkin et al., 2016). Some experiments with tilted lidars were carried out (Del Guasta et al., 2006; Hayman et al., 2012, 2014; Neely et al., 2013, Veselovskii et al., 2017) and showed a high probability of the presence of oriented particles.

Comment 2

Pg 2, Line 54. In this paragraph the authors cite several works stating that these works observed both horizontal orientation and azimuthal orientation. This is not true. Most of the references make no mention of observing azimuthally oriented ice crystals which implicitly seems to suggest they didn't observe any. There are a few works (such as Kaul 2004 and Balin 2011) that do mention observing this effect. Beyond that I happen to know number of the researchers cited are very skeptical about the existence of of azimuthally oriented ice crystals outside of thunderstorms. I doubt they would appreciate being *cited in support of this claim. The authors need to accurately represent the results of prior work and most of the citations used here do not support the statement or even contradict the statement.*

Response

Indeed I put this phrase very incorrectly. Sorry, I mistakenly cited some authors who did not mention the azimuthal orientation.

I reason like this. If azimuthal orientation takes place, the parameters of the backscattered radiation depend on the orientation of the lidar reference plane relative to the direction of the preferential orientation of particles. *Direct measurements* of azimuthal orientation should be carried out as follows. We set lidar vertical and use linear polarized radiation. If the lidar reference plane coincides with the direction of the action of the orienting factor, the matrix of this cloud will have a block form

$$\mathbf{M} = \begin{vmatrix} m_{11} & m_{12} & 0 & 0 \\ m_{12} & m_{22} & 0 & 0 \\ 0 & 0 & m_{33} & m_{34} \\ 0 & 0 & -m_{34} & m_{44} \end{vmatrix}$$, (Kaul, 2000). Then we rotate the lidar around a vertical axis. One can easily show (Kokhanenko et al., 2018) that signal energy $E^{lin} = m_{11} + m_{12}\cos 2\varphi$ depends on the angle of rotation of the lidar relative to the plane of preferential orientation of the particles in the cloud if $m_{12} \neq 0$. According to a large array of experimentally measured BSPM (Kaul et al., 2004), the average value of $m_{12} = -0.22$. The distributions of relative frequencies for m_{12} shows the probability that the value of m_{12} lies in the interval [-0.6, -0.3] is approximately equal to 30% (Kaul et al., 2004, Balin et al. 2009). Therefore we would have to observe the modulation of the signal very often.

The density of the cloud can change during the time of rotation. The signal from circular polarization serves as a reference for tracking changes in the signal that are not related to the rotation of the lidar. The function $F(\varphi) = \dfrac{E^{lin}(\varphi)}{E^{circ}(\varphi)} = 1 + \dfrac{m_{12}}{m_{11}}\cos 2\varphi$ varies with a period of 180° and one of the extremes of this dependence (max or min, this depends on the sign of the element m_{12}) coincides with the position of the plane of symmetry. However, authors are unaware of such direct measurements. Because our lidar (i) can scan around vertical axes, and (ii) measures both linear and circular polarization, we can make observations using this technique. It is unfortunate, but all the measurements we carried out to date, have not shown the presence of azimuthal orientation. We plan to continue such observations in the future.

Indirect evidence of the existence of a preferential azimuthal orientation can be obtained from the form of measured BSPM. Instead of lidar rotation we can transform the matrix using the rotation matrix R(φ) to the plane of symmetry. If the matrix may be represented in the block form, this suggests a high probability of the presence of a fraction of oriented particles (Kaul 2000, Kaul et al. 2004, Samokhvalov et al. 2014). In a similar manner Hayman et al., 2014 simulated the rotation of measured matrix and made a conclusion about the orientation of the particles based on the change of the calculated depolarization ratio.

References to add:

Kokhanenko, G.P., Balin Yu.S., Borovoi A.G., Klemasheva M.G., Nasonov S.V., Novoselov M.M., Penner I.E., Samoilova S.V. "Investigations of the crystalline particle orientation in high-level clouds with a scanning lidar," ", Proc. SPIE 10833, 24th International Symposium on Atmospheric and Ocean Optics: Atmospheric Physics, 1083347 (13 December 2018); https://doi.org/10.1117/12.2504129

Samokhvalov, I.V., Nasonov, S.V., Stykon, A.P., Bryukhanov, I.D., Borovoi, A.G., Volkov, S.N., Kustova, N.V., and Konoshonkin, A. V., "Investigation of phase matrices of cirrus containing ensembles of oriented ice particles," Proc. SPIE 9292, 20th International Symposium on Atmospheric and Ocean Optics: Atmospheric Physics, 92922M (25 November 2014); doi: 10.1117/12.2075562

Revised text

Particle orientations are promoted not only by aerodynamic forces, but also by forces of a different nature, such as wind shifts and electric fields. Kaul 2000 supposed that in such conditions, crystalline particles can have a preferential orientation in the horizontal plane (azimuthal orientation). It is obvious that the direction of preferential orientation is connected with the direction of action of these forces. The basis for such conclusion is the observed non-invariance of the BSPM with respect to rotation of the coordinate system (Kaul 2000, Kaul et al. 2004, Samokhvalov et al. 2014, Hayman et al., 2014). If we use linear polarized radiation and rotate the lidar around a vertical axis, signal energy depends on the angle of lidar rotation relative to the plane of preferential orientation of the particles if $m_{12} \neq 0$ (Kokhanenko et al., 2018). According to a large array of experimentally measured BSPM, the distribution of relative frequencies for m_{12} shows that the value of m_{12} lies in the interval [-0.6, -0.3] with the probability about 30% (Kaul et al., 2004, Balin et al. 2009). Therefore we would have to observe the modulation of the signal very often. However, authors are unaware of such direct measurements.

Discretionary Edits

Comment 3.

...The authors should be careful about overasserting what their observations definitively prove about the scattering volume. . (Pg. 8 starting on line 235)... In that context, the authors later assert that the depolarization values are indicators for the relative mass of oriented and randomly oriented ice (Pg. 10 line 284). .....

Response

Your comments are very useful, and I will try to take it into account when finalizing the text. As for line 284, I try to revise this text

Revised text

pg.10, Line 302

the ratio $\left(I_{\parallel}\left(0°\right)-I_0\right)/I_0$ may reflect the contribution of mirror particles to the lidar signal.

Comment 4.

Pg 11, Line 316 "... including exploring the azimuthal orientation of particles." I suggest being clear that this was not explored in the current work and that looking for azimuthal orientation of particles would be in future work.

Response

I slightly changed the text

Revised text

pg.11, Line 331

Since the circular polarization signal does not depend on the rotation of the lidar relative to the direction of particle orientation, this polarization can be used as a reference for investigation the azimuthal orientation of the particles.

Comment 5.

Pg 3, Line 62-64 It is not clear how the authors come to the conclusion that m12=-0.22 +/ -0.2 means that in 30% of the observational cases, the depolarization depends on the lidar reference plane. The value of m12 certainly does not dictate this. Is the assumption that PDF of m12 is Gaussian?

Pg 3, Line 64 "In other words: : :" This statement isn't totally clear. I think to clarify you want to say "...when the lidar's linear polarization rotates around: : :"

Response

See the response to comment 2

Comment 6.

With regard to the near range channel, I'm a little confused about what its purpose is. Doesn't the fiber scramble the polarization modes and therefore prevent measurement of the depolarization ratio with this channel? What is this channel being used for? What ranges are the near and far range channels used for?

Added text

pg.4, Line 124.

The small receiver is closer to the transmitter, so the transition to range-square mode starts earlier (80-100 m) than for the large receiver (800-900 m). During data processing signals from near zone (50-1200 m) and far zone (400 m-15 km) fit together at a distance of 800-900 m when range-square mode for large receiver starts. Of course, the optic fiber destroys the polarization state of the signal, so near-zone data cannot be used for polarization analysis.

Comment 7.

Pg. 10 Line 278. The authors state that the signal variations with angle are smaller than the measurement errors. This really depends on what the authors mean by "measurement errors" because one can clearly see a trend in the data, so the limiting *factor does not appear to be random error. If they mean this is less than the systematic error of the instrument, this is certainly a valid point. It would be good to clarify which type of errors they are referring to.*

Also with regard to Figure 10 and the perpendicular measurements, I wonder if this angle dependence is the result of cross talk between the channels. Perhaps this is what the authors are referring to as "measurement error". If so it would be helpful to simply state that explicitly.

Response

Analysis of measurements errors is very difficult. As for "cross talk", I suspected that this is so, but I did not know how to express it.

Revised text

pg.10, Line 293.

Cross-polarized signals $I_\perp$ have random variations from pulse to pulse comparable with the average value. In most cases the values of $I_\perp$ show a weak decline of intensity with the angle, but these variations do not exceed instrumental errors (about 1% for depolarization ratio). Figure 10a shows the variations even less the 0.5%. Moreover, a slightly noticeable maximum at α=0° looks like signal penetration from parallel to perpendicular channel. Therefore we think, than linear trend is not statistically reliable. We can conclude that $I_\perp$ is practically independent of the tilt angle.

Comment 8.

Pg. 10, Line 300 The authors describe that the depolarization measurements at 532 nm are only made for linear polarizations. This needs to be better explained in section 2 Lidar Description. I had assumed (incorrectly) that the authors were using a dual wavelength wave plate. Make it clear what wavelengths the polarization optics are designed for and please be clear throughout the manuscript that this instrument performs the two polarization measurements only at 1064.

Response

The measurements for linear polarization can be made simultaneously for two wavelength 532 and 1064 nm. As for circular polarization, it is depend on the installed quarter-wave plates. Experiments described in the article were made with the plate, designed for 1064 nm. We can use a quarter-wave plate for 532 nm if it is planned. Similar we change a half-wave plate (532 or 1064nm) for calibration.

Revised text

pg.4, Line 107.

We have two sets of quarter-wave plates. One set is designed for 532 nm, another set for 1064 nm. For the wavelength of installed plates (below are the results only for installed 1064 nm plates) we can investigate both linear and circular polarizations. For the second wavelength (532 nm) polarization state when turning 45 degrees is not determined. However, in the position where the axis of the rotating phase plate coincides with the plane of polarization of the transmitter, the radiation remains linearly polarized for any wavelength. So the measurements for the wavelength of λ = 532 nm were carried out only for linear polarization of radiation. Of course, in our lidar we can use a quarter-wave plates for 532 nm if such experiments were planned.

Response to Referee #2

Comment 1

"Clouds of Upper Layers" in the title sounds strange. It would be better to replace it with "ice clouds" or "clouds in the upper troposphere". Why you mention "upper layers", you can as well observe clouds and ice clouds in lower parts of the troposphere. In general, I would omit the term "upper layers" throughout the whole manuscript. It can be replaced by "upper troposphere".

Response

I agree that the term "layer" is incorrect and very unfortunate. The terms "High-level" or "Mid-level clouds" are recommended by the International Cloud Atlas. I will try to use these terms in the manuscript and "ice clouds" in the title.

Comment 2

I miss a bit the discussion about the atmospheric relevance of your findings. What does the additional information we get by scanning through the cirrus help us in characterizing cirrus clouds? It is interesting to know, if a cirrus cloud consists of orientated or randomly orientated ice crystals. In the introduction you mention the sun glare. You could add discussion about the atmospheric implications of your findings. This will further underline the importance of your newly developed lidar system.

Response

I can only say that both the shape of the crystalline particles and the presence of their orientation are determined by complex meteorological processes in the cloud. Therefore, the study of the orientation of crystalline particles provides significant information about these processes. However, the authors are not experts in the field of cloud physics. So I would not like to open a big discussion on this issue

Revised text, Line 75. The optical properties of ice clouds, including their effect on the radiation balance, are determined by both the microphysical properties of crystalline particles and the presence of their orientation. These properties are in turn determined by complex meteorological processes in the clouds. Therefore, the study of the orientation of crystalline particles provides significant information about these processes.

Comment 3

You give an exponential parameterization (equation 1). But the reader finds nowhere in the manuscript any parameters for this fit. You should definitely provide some fitting parameters for your curves (A, alpha_0, w).

Response

It's not quite so.

Line 317. (in the revised text) For Fig. 10a w=42 arc minutes, for Fig. 10b w=82′.

Line 330. For all measurements the value w is within 40-160 arc minutes.

Values w are indicated in *Fig. 11* with squares. (Fig 11 and other figures is corrected)

Line 330. The shift α_0 of the curve maximum from 0° is less than 2 minutes, (a symbol "α_0" is added into the text). The absolute values A and I_0 are not interesting, because they are determined by the sensitivity of photodetectors. The ratio $I(0°)/I_0$ is indicated in Fig. 11.

Comments 4, 5, 6

4. To discuss the differences in the cirrus observations, it would be extremely helpful to provide some more information about the cirrus cloud. Firstly, the temperature profile within the cirrus. You show some radiosonde data in Fig. 7+8, but you don't use this information in the text. At which temperature do you observe the two cirrus clouds on 6 April 2018? At colder temperatures, the ice crystals may have different properties. To improve the Figures, I would show a temperature profile exactly for the same height range (6 – 10 and 7.5 – 12 km) as in Fig. 7a+b and 8a+b instead of the shown diagram. And please add the time of radiosonde launch.

Secondly, the different exponential behaviors in Fig. 11 are related to different cirrus clouds. What additional information do you have about these cirrus clouds? Cloud height? Cloud thickness? Cloud top temperature? Temperature profile within the cloud? Age of the cirrus cloud? Formation process? May this information help to explain the different behavior?

5. Where did you perform the measurements? In Tomsk. Can you add some coordinates? How far was the radiosonde station?

6. How did you select the measurements in Fig. 11 (ln 280)? Which criteria did you use?

Response

I agree that radiosonde data should be presented more clearly. But we do not know the meteorological parameters of each layer inside the cloud. It is because of the distant location of the station and the rare launches of probes (once every twelve hours). Clouds change their structure in 5-10 minutes. No radiosondes can provide such volatile information. Then, our previous observations (Balin 2011) showed that mirror layers may exist in both the lower and upper parts of the cloud. So the layer height inside the cloud also does not correlate with its polarization. The selection of cloud portions presented in the figure 11 is rather random and subjective. The only requirement is: these portions must have a pronounced dependence on the tilt angle, and there is no signal overflow when the lidar is oriented to zenith (Sect. 4.2). Today I don't know how to proceed and present the data (polarization) across all cloud height.

Revised lines in the text

Line 252. Measurements were made in Tomsk (56°28'N, 85°E)

Line 270. Radiozonde sounding was carried out at Novosibirsk station, about 250 km from Tomsk to SW, two records were made at 07:00 and 19:00 LST. Of course, due to the distant location of the station and the rare launches of probes (once every twelve hours) these data do not describe the fine structure of the ice cloud.

Line 275. A high-level cloud consists of two layers. The thin bottom layer (6600-7000 m) has a temperature minus 26-31°C, the top layer (7800-9800 m) temperature is 37-52°C below zero

Line 287. A cirrus cloud with a complex structure extends in a layer of 8 - 11.7 km. The temperature in the cloud varies from -34°C to -60°C.

Line 325. Figure 11 gives some selected dependences of intensity angle distributions for component $I_{\parallel}$. We did not find any correlation of the distribution parameters (A, I_0, w) with the height of the selected area inside the cloud. So the selection of cloud portions presented in Fig. 11 is rather subjective. The only requirement is: these portions must have a pronounced dependence on the tilt angle, and there is no signal overflow when the lidar is oriented to zenith.

Comment 7

The symbols â´L˘e and âŁ˘e correspond to parallel and orthogonal normally linked to linear polarization. Circular polarization is right handed or left handed or more general it can be described as co-polar and cross-polar. Or at least mark the intensity as a circular polarized component whenever it is used to not confuse the reader with the linear polarization.

In general, you should be more careful in distinguishing the linear and circular depolarization ratio throughout the text (often it is just stated "depolarization ratio").

Response

I suppose that left-handed and right-handed circular polarizations are orthogonal, too. But I agree that the use of a symbol $I_{\perp}$ may be unreasonable for circular polarization. So I will use I_{co} and I_{cros} in the text and figures. Then the depolarization ratio is equal to I_{cros}/I_{co} both for linear and circular polarization.

Comment 8

The paragraph line 286-292 describing the relation of circular and linear polarization should be placed earlier. The same holds for the information in line 300-303. Till these lines, it remained unclear how you deal with two wavelengths and a quarter wave plate. This has to be mentioned when describing Fig. 4.

Response

Lines 300-303 are now in Sect.2. Lines 286-292 are shifted to the beginning of Sect. 4.1.

Revised text

Line 111. We have two sets of quarter-wave plates. One set is designed for 532 nm, another set for 1064 nm. For the wavelength of installed plates (below are the results only for installed 1064 nm plates) we can investigate both linear and circular polarizations. For the second wavelength (532 nm) polarization state when turning 45 degrees is not determined. However, in the position where the axis of the rotating phase plate coincides with the plane of polarization of the transmitter, the radiation remains linearly polarized for any wavelength. So the measurements for the wavelength of λ = 532 nm were carried out only for linear polarization of radiation. Of course, in our lidar we can use a quarter-wave plates for 532 nm if such experiments were planned.

Comments 9,10

Figures and captions.

All figures and captions are updated

Comment 16

ln 89 “to evaluate some elements of BSPM” Which elements? Be more precise

Revised text

Line 94. ...that makes it possible to detect the deviations of BSPM from diagonal shape (Balin et al., 2011).

Comment 18

ln 94 “PP1 with the phase shift of 20 wavelengths is used for _ = 532 nm, and 9.5 wavelengths for _ = 1064 nm.” What do you mean by this?

Revised text

Line 98. For coincidence of the polarization planes, the phase plate *PP1* with the phase shift of 20 wavelengths for $\lambda = 532$ nm and 9.5 wavelengths for $\lambda = 1064$ nm is installed. The rotation of this plate causes the rotation of the polarization plane for 1064 nm but does not affect the polarization of 532 nm.

Comment 21

ln 146 Where do you get this value from?

Revised text

Line 160. Accuracy of installation angle is $\theta=34'=0.0125$ rad. ... θ is a small setting angle error. $\Delta\delta=\theta^2=0.000156\approx0.016\%$

Comment 22

*ln 148-150: 45_ * 0.68 ms /0.3_ = 102 ms Using the information you provided, the quarter wave plate would need 102 ms to turn by 45_. That would be too slow for a laser repetition rate of 10 Hz. Maybe you just have to report one more significant digit for time?*

Response

I think, 102 ms is not much different from 100 ms need for 10Hz repetition rate. I have already inserted next lines into the text.

Line 133. The rotation of the mirror obturator and platforms with phase plates is synchronized with the external trigger of the laser. So laser pulse frequency is about 10 pulse per second, but its exact value is determined by the obturator controller.

Comment 23

ln 157-158 Here it would be helpful to already mention Fig. 5. Otherwise, the number of steps seems somehow arbitrary

Response

This is a very interesting offer.

Comment 24,25

24. Fig. 5a Why do you show this plot?

25. ln 159-164: The same procedure is done for plate B without plate A, isn't it?

Revised text

Line 175. The rotation angle setting is monitored by the zero position sensors of platforms. When installing the plates in the platform frame, the plate axis can be shifted relative to the sensor at a certain angle, initially unknown. However, a laser pulse must be produced at the moment when the axis of the plates coincides with the reference plane of the lidar. The exact positions of the plates in the frame is set separately for plate A and B. We set one plate (e.g. plate B) in its channel (receiver for plate B) and turn on the rotation. A section of a homogeneous atmosphere with small aerosol content is selected. Figure 5a shows the lidar signals from two photodetectors (P_{co} and P_{cros}), summarized over all positions of plate B (red and green lines). A height range from 6 to 9 km was chosen, on which the depolarization ratio (blue line) is constant.

For each pulse, the rotation angle of the plate was recorded and the average value of the depolarization ratio over the range of 6–9 km was calculated. These values are shown in Fig. 5b (bottom frame). The dependence averaged over 30 minutes is shown in the upper frame in Fig. 5b. Minimal depolarization is observed at the 34th step of the platform. The accuracy of platform setting is ± 1 step, which corresponds to 0.03% error with respect to depolarization ratio. Similar adjustment of the plate A gives an exact position at the 45^{th} platform step.

A timing diagram in Fig. 4b shows the position of the laser pulses relative to the zero position of the plates. 31 ms interval (45 steps) for plate A and 23 ms (34 steps) for plate B passes before the first laser pulse. The situation repeats every 8 pulses. As already mentioned, the frequency of laser pulses is strictly synchronized with the rotation of the plates.

Comment 29

ln 220 The calibration was made 7 May 2017, the measurements are performed one year later. Did you perform calibration measurements in 2018 as well? What can you say about the stability of such calibration measurements?

Response

Of course, Similar calibration procedures were carried out before measurements in April and June 2018. I will clarify the values of these constants.

Revised text

Fig. 7b shows the value of calibration constant *K,* calculated in the height range of 1800-8000 m. In this case, the mean value *K*=1.91. Similar calibration procedures were carried out before each measurement in April and June 2018. All values *K* did not deviate by more than ±0.05.

Comment 32

Why do you study the range -1 to 4_ only? Many lidar systems are operated at an off-zenith angle at 5_. It would be interesting to extend your tilt angle up to 5_, even if the change from 4_ to 5_ will not be significant.

Response

The most interesting is a scanning over 30° when the polarization from oriented plates changes abruptly. But due to the inhomogeneities of ice clouds scanning should be done in a short time. We chose a small scanning angle for this reason. I think in future measurements we will use a wider angle. May be the scanning from -5 to +5 will be used, because the symmetry around vertical position, I suppose, can indicate cloud uniformity. And certainly the scanning around 30° is interesting.

Comment 33

ln 250 "Values outside the vertical are close throughout the entire cloud thickness." – Close to what?

Response

Values δ^{Circ} outside the vertical are close to 100% throughout the entire cloud thickness.

Comment 36

ln 273 How to determine I_0 (for alpha » 4_) if the scanning cycles are only done up to 4_?

Response

Certainly, I_0 is obtained by fitting the function by the least squares method. But it is better to remove (a>>4) from the text.

Revised text

Line 315. I_0 is the offset of dependence determined by a signal without the specular component

Comment 37,47

37. ln 278-279 Can you provide a mean and a standard deviation? Or maybe add it as a dashed line in Fig. 10.

47. Fig. 11 You just show some fitting results without showing the original data points. Can you underlay your fitting curves (in bold) with the data points in the corresponding color (in a light hue). Then, the reader will see the data used for these fits.

Response

I think that the scatter of experimental data for single pulses well demonstrates approximation errors. I added data points to Fig. 11

Comment 39

ln 305 "thus, the amplitudes of signals are reduced to one value" – How?

Revised text

Line 345. The relative sensitivity of photodetectors at 532 and 1064 nm was not calibrated. Therefore the intensities of polarization components for 532 nm (both I_{co}^{Lin} and I_{cros}^{Lin}) were normalized so that the intensity maximum of I_{co}^{Lin} (0°) in the vertical position coincided with I_{co}^{Lin} (0°) for 1064 nm.

Response to Referee #3

Experiment

Comment 1

Lines 114 f.: Please, provide more information about the fiber (polarization preserving?) and the shutter (coating?).

Revised text

Line 127. The signal from the receiver of the near range through the optic fiber *Fb* is fed to the mirror shutter (aluminium coated obturator) *MS* , by means of which the signals of the near and far ranges are alternately switched. The small receiver is closer to the transmitter, so the transition to range-square mode starts earlier (80-100 m) than for the large receiver (800-900 m). During data processing signals from near range (50-1200 m) and far range (400 m-15 km) fit together at a distance of 800-900 m when range-square mode for large receiver starts. Of course, the silica optical fiber (1 mm diameter) destroys the polarization state of the signal, so near-range data cannot be used for polarization analysis.

Comment 2

How is background scattering suppressed? There seem to be no filters in the setup, is this correct?

Response

Of course, we use interference filters before each detector. They are depicted in Fig. 2 as narrow rectangles, but were not mentioned in the text.

Revised text

Line 149. Interference filters (*IF*) with bandwidth about 1 nm are placed in front of the detectors.

Comment 3

Lines 149-150: 150 Steps are required for a 45_-turn, which would take 102 ms (according to the information provided) and thus slightly longer than the time period between the 10-Hz laser pulses. Please, comment.

Revised text

Line 133 - The rotation of the mirror obturator and platforms with phase plates is synchronized with the external trigger of the laser. So laser pulse frequency is about 10 pulse per second, but its exact value is determined by the obturator controller.

Comment 4

Lines 159-160: ‘Only one: : : channel’. Please, provide more details.

Revised text

Line 177 - The exact positions of the plates is set separately for plate A and B. We set one plate (e.g. plate B) in its channel (receiver for plate B) and turn on the rotation.

Measurements

Comment 1

Lines 242 ff.: It is not obvious what is meant with 'double lines'.

Revised text

Line 283 - In Fig. 7a we saw clearly expressed single line of maximum signal, because the vertical position was the edge position when scanning. When we scan our lidar from 4° to -1° and back, vertical positions (0°) are close to each other. So in Fig. 8a two lines of maximum signals are close to each other and look like a double line.

Comment 2

Line 264: Figs. 7-9 present data from April and June, 2018. Then, suddenly, 1 October is mentioned. Please, provide earlier on in the section an overview of the measurements to be discussed.

Response

It is a mistake. October 1 is not need here. Below we present the data obtained on 2 June.

Comment 3

Paragraph, lines 286 ff.: This information must be provided before the measurement are presented, because otherwise the interested reader is waiting for the linear depolarization ratios to be shown.

Response

Thank you, I moved this lines to the beginning of Sect. 4.1

Comment 4

Paragraph, lines 300 ff.: This information definitely belongs to section 2 or 3!

Response

This lines are moved to Sect. 2 and clarified

Revised text

Line 111. We have two sets of quarter-wave plates. One set is designed for 532 nm, another set for 1064 nm. For the wavelength of installed plates (below are the results only for installed 1064 nm plates) we can investigate both linear and circular polarizations. For the second wavelength (532 nm) polarization state when turning 45 degrees is not determined. However, in the position where the axis of the rotating phase plate coincides with the plane of polarization of the transmitter, the radiation remains linearly polarized for any wavelength. So the measurements for the wavelength of λ = 532 nm were carried out only for linear polarization of radiation. Of course, in our lidar we can use a quarter-wave plates for 532 nm if such experiments were planned.

Phrasing

Comment 4

Lines 186-188: 'If: : : sounding.'

Revised text

Line 211. The channel calibration problem is solved in most devices for polarization measurements. An exception is devices where signals of different polarization are sequentially directed to one photodetector (Platt, 1977; Eloranta and Piironen, 1994; McCullough et al., 2017).

Comment 6

Line 305: 'thus: : : value.'

Revised text

Line 345. The relative sensitivity of photodetectors at 532 and 1064 nm was not calibrated. Therefore the intensities of polarization components for 532 nm (both I_{co}^{Lin} and I_{cros}^{Lin}) were normalized so that the intensity maximum of I_{co}^{Lin} (0°) in the vertical position coincided with I_{co}^{Lin} (0°) for 1064 nm.

Typos

Comment 3

Line 66 'The authors', ***full stop missing***

Response

We did not quite understand what does this means, so I've replaced the sentence:

Revised text

Line 67. However, we did not find references to such direct experiments in the literature.

Figures.

I substantially reworked all the figures and their captions in accordance with the comments of the reviewers.

References and typos.

Thank you for your comments. Your remarks were very helpful. We tried to take everything into account in the revised text.

Response to Referee #4

Comment 1

Provide a full description of the various symbols in Figure 2, in the caption of the figure.

Response

I expanded the caption to the figure

Revised text

Figure 2. Optical circuit of the LOSA-M3 lidar. PP: phase plates; GP: Glan prism; BE: achromatic beam expander; AL: achromatic lens 40 mm diameter; CL: Cassegrain mirror lens *CL* 200 mm diameter; VC: video camera; FS1, FS2: iris diaphragms; Fb: optic fiber; MS: mirror shutter; L: lense; WP: Wollaston prism; BS: beamsplitters; APD: avalanche photodiodes; PMT: photomultiplier tubes.

Comments 2,3

2.Provide a full description of the measurement sequence, in terms of the measurements at near and far zones, measurements at different wavelengths, measurements with linearly- and circularly-polarized emission (and corresponding detection), so the sequence of the measurements and their time resolution is clear. The use of a new figure to provide this sequence visually would help.

3. The system relies heavily on its rotating parts, but in the text there is not much information about their synchronization. Please provide your comments on this and/or the tests you performed to check for this.

Response

I think that the addition of a new figure is difficult, since there are already 13 figures. Some information about the synchronization of laser pulses and plate rotation is shown in Figs. 4, 6.

I have reworked some pieces of the text related to the obturator and phase plates where the alternation of near and far ranges is described.

Revised text

Line 134. Shutter controller sets the obturator rotation frequency, the rotation speed of the phase plates and externally triggers the laser. So laser pulse frequency is about 10 pulse per second, but its exact value is synchronized with the rotation of the mirror obturator and platforms with phase plates.

There may be times when we are only interested in distant objects, such as high-level clouds. In this case, the obturator's rotation speed doubles, and the laser only starts when the shutter is open. The frequency of the laser pulses remains the same (10 Hz), but only far range signals are recorded.

Line 195. The diagrams indicated in Figs. 4, 6 refer to the cases of registration only the far range signals. If we register both near and far range signals, the plates rotate through the angle 22.5° between laser pulses. Intermediate positions correspond to the near range signals and have an undefined polarization.

Some more comments:

Comment 1

Make Fig. 4a and 4b two different figures. It is confusing to be in the same figure, because the first refers to the rotation of the phase plates and the second refers to the definition of their initial position.

Response

This is a reasonable offer. Moreover, in the last version of the text (uploaded 28 Oct) I first refer to Fig. 4a, then Fig 5, and then 4b. Therefore now Fig. 4b will be Fig. 6.

Comment 2

Change caption of Fig. 5a to "lidar signal used to mount the plates at their initial position"

Response

Now the caption of Fig. 5 is:

Revised text

Figure 5. (a) Lidar signals from two photodetectors (P_{co} and P_{cros}), summarized over all positions of plate B (red and green lines). A height range 6-9 km with constant depolarization ratio (blue line) is chosen to adjust the plates. (b) Depolarization ratio for each pulse (bottom) and averaged over a 30 minute record (top).

I believe that the new caption takes into account the need to show the lidar signal in the figure 5a.

Scanning polarization lidar LOSA-M3: opportunity for research~~the possibility~~ of ~~studying the~~ crystalline particle orientation in the ice~~upper layers~~ clouds

Grigorii P. Kokhanenko, Yurii ~~.~~S. Balin, Marina G. Klemasheva, Sergei V. Nasonov, Mikhail M. Novoselov, Iogannes E. Penner, Svetlana V. Samoilova

V.E.Zuev Institute of Atmospheric Optics~~,~~ SB RAS, Tomsk, Russia

Correspondence to: Grigorii Kokhanenko (kokh@iao.ru)

Abstract. The article describes a scanning polarization lidar LOSA-M3, developed at the V. E. Zuev Institute of Atmospheric Optics, the Siberian Branch of Russian Academy of Sciences (IAO SB RAS). The first results of studying ~~investigation of~~ the crystalline particles orientation by means of ~~carried out with~~ this lidar are presented herein. The main features of LOSA-M3 lidar are the following: 1) an~~-~~ automatic scanning device~~drive~~, which allows to change the sensing direction ~~of sounding with~~in the upper hemisphere at the ~~a~~ speed ~~of~~ up to 1.5 degrees ~~degree~~ per second with the accuracy of ~~the set~~ angle measurement setting at least ~~no worse than~~ 1 arc ~~angle~~ minute; 2) ~~) the~~ separation of ~~the~~ polarization components of the received radiation is carried out directly behind the receiving telescope, without installing the elements distorting ~~the~~ polarization, such as ~~of the elements~~ dichroic mirrors and beamsplitters; and 3)~~)~~ continuous alternation ~~from pulse to pulse~~ of the initial polarization state (linear - circular) from pulse to pulse that~~which~~ makes it possible to evaluate some elements of the scattering matrix.

For testing lidar performance several~~Several~~ series of measurements of the ice~~upper layer crystalline~~ cloud ~~polarization~~ structure in the zenith scan mode were carried out in Tomsk in April-June~~October~~ 2018. The results show that the degree of horizontal orientation of ~~the~~ particles can vary significantly in different parts of the cloud. The dependence of ~~the~~ signal intensity on the tilt angle ~~of inclination~~ reflects the distribution of ~~the~~ particle deflection relative to the horizontal plane, and is well described by the exponential dependence. The values of cross-polarized component in most cases show~~shows~~ a weak decline of intensity with the angle. However, these variations~~, but its change~~ are smaller than the measurement errors. We can conclude that it is practically independent of~~on~~ the tilt~~inclination~~ angle. In most cases the ~~The~~ scattering intensity at the~~a~~ wavelength of 532 nm has a wider distribution than at 1064 nm.

1 Introduction

Cirrus clouds cover a significant part of the earth's surface. Thus, they~~They~~ have a significant impact on the radiation balance and climate, primarily due to the effects of radiation attenuation and reflection ~~of radiation~~ (Liou, 1986; Sassen et al., 1989). In many cases, crystalline particles of cirrus clouds have a pronounced orientation in space. This leads to optical anisotropy, manifested in various forms of the solar halo. Anisotropy affects the passage and reflection of radiation from clouds and, for example, leads to ~~a~~ dependence of ~~the~~ reflectivity on the zenith angle of the sun (~~Lavigne et al.,2008;~~ Klotzsche and Macke, 2006; Lavigne et al., 2008).

The most well-known phenomenon is a ~~the~~ predominant orientation of ~~the~~ crystals in the horizontal plane. It can be caused by aerodynamic forces arising from the free fall of particles (Kaul and Samokhvalov, 2005). Sections~~Sites~~ with the ~~a~~ horizontal orientation of ~~the~~ particles manifest~~are manifested~~ in ~~the~~ occurrence of sun glare when observing cloud cover from space (Chepfer et al., 1999; Masuda and Ishimoto, 2004). Analysis of the glare width ~~of the glare~~ shows the correspondence to the Gaussian distribution of ~~the~~ crystal inclination~~slopes~~ with the ~~a~~ half-width ~~of~~ about 0.4 degrees (~~Lavigne et al.,2008;~~ Breon and Dubrulle, 2004; Lavigne et al., 2008). Presence~~). The presence~~ of horizontally oriented crystals is also detected when observing specular spots from the ~~a~~ spotlight on the clouds (Borovoi et al., 2008);~~),~~ flutter width is also estimated at 0.4°. Lidar~~However, lidar~~ observations of the ice ~~crystalline~~ clouds provide the basic information about ~~the~~ particle orientation (Platt et al., 1978; Chen et al., 2002; Noel and Sassen, 2005). ~~; Chen et al., 2002).~~

Unlike water clouds, ice ~~crystalline~~ clouds cause greater depolarization of ~~the~~ backscattered radiation (Sassen and Benson, 2001). Most often, ~~the depolarization ratio is within $\delta = 0.3$–0.6~~ in the cloud areas ~~of a cloud~~ with randomly oriented particles~~, the depolarization ratio is within $\delta = 0.3$–0.6~~ (Noel et al., 2002; You et al., 2006). The magnitude of ~~the~~ depolarization is undoubtedly related to the shape of ~~the~~ particles and the phase composition of ~~the~~ cloud, which are ~~is~~ taken into account when analyzing the observations of cirrus clouds (Noel et al., 2002; Hoareau et al., 2013; Campbell~~Stillwell~~ et al., 2015~~2018~~; Haarig et al., 2016; ~~Stillwell~~Campbell et al., ~~2018~~2015).

Starting from the works of Sassen, 1977 and Platt et al., 1978 ~~and Sassen, 1977,~~ numerous observations show that with a ~~the~~ vertical orientation of the lidar, the horizontally oriented particles cause a specular reflection, manifested in the absence of depolarization and increased backscattering (~~Sassen and Benson, 2001; Sassen, 1991;~~ Platt, 1978; Thomas et al., 1990; Sassen, 1991; Sassen and Benson, 2001). Data analysis of the polarization lidar in the CALIPSO experiment (Cho et al., 2008; Noel and Chepfer, 2010; Yoshida et al., 2010) shows that a significant fraction of horizontally oriented particles in mid~~middle~~ latitudes is observed in the temperature range from -35°C to -5°C. Deviation of the lidar from the vertical position eliminates the effect of mirror reflection. For example, the CALIPSO lidar is ~~deflected at~~ 3° deviated from the nadir to eliminate this effect (Hunt et al., 2009). The angular dependence of ~~the~~ depolarization may vary for clouds with different temperatures (Sassen and Benson, 2001; Noel and Sassen, 2005~~; Sassen and Benson, 2001~~). According to ~~the~~ data from ~~of~~ these works, the dependence of ~~the~~ signal amplitude on the lidar tilt angle corresponds to the Gaussian distribution.

Another effect caused by the horizontally oriented plates and columns is the ~~a~~ corner reflection. It appears when the lidar is tilted at a significant angle. Depolarization of backscattered radiation has a maximum at a lidar tilt of~~inclined~~ 30 degrees for oriented plates and about 60 degrees for columns (Borovoi et al., 2000). A more detailed simulations show that when angular reflection is taken into account, the element a_{44} of the light backscattering phase matrix (BSPM) is most informative in determining of the flutter~~° from the zenith~~ (Konoshonkin~~ et al.~~, 2016). For the plates, an abrupt change in the a_{44} occurs at a tilt angle of 30 degrees, while for the columns this element begins to grow smoothly at 30 degrees and reaches a maximum at 60° (Konoshonkin et al., 2016). Some experiments with tilted lidars were carried out (~~Experiments with tilt angles of 30-43° were carried out (Hunt et al., 2009;~~ Del Guasta et al., 2006; Hayman et al., 2012, 2014; Neely et al., 2013,~~;~~ Veselovskii et al., 2017~~; Neely et l., 2013~~) and showed a high probability of the presence of oriented particles.~~such an effect.~~

Particle orientations are promoted not only by aerodynamic forces, but also by forces of a different nature, such as wind shifts and electric fields. Kaul, 2000 supposed that in such conditions, crystalline particles can have~~. A number of works on polarization sounding of cirrus clouds (Chepfer et al., 1999; Noel and Sassen, 2005; Hayman et al., 2012; Kau et al., 2004; Balin et al., 2011; Borovoi et al., 2014; Hayman et al., 2014) showed that crystalline particles often demonstrate not only a preferential orientation relative to the horizon (zenith orientation) but also~~ a preferential orientation in the horizontal plane (azimuthal orientation).~~ The probable reasons for this orientation are wind shifts and electric fields.~~ It is obvious that the direction of preferential orientation is connected with the direction of action of these forces~~ (Kaul, 2000)~~. The basis for such ~~a~~ conclusion is the observed non-invariance of the ~~light backscattering phase matrix (~~BSPM~~)~~ with respect to ~~the~~ rotation of the coordinate system (Kaul, 2000; Kaul et al., 2004; Hayman et al., 2014; Samokhvalov et al., 2014). If we use linear polarized radiation and rotate the lidar around ~~or the cloud as~~ a vertical axis, signal energy depends on the angle of lidar rotation relative to the plane of preferential orientation of the particles if ~~whole). For example, according to a large array of experimentally measured BSPM (Kaul et al., 2004) the zero value of the element~~ m_{14} (Kokhanenko et al., 2018). According to a large array of experimentally measured BSPM, the distribution of relative frequencies for m_{12} shows that the value of m_{12} lies in the interval [-0.6, -0.3] with the probability about 30% (Kaul et al., 2004; Balin et al., 2009). Therefore we would have to observe the modulation of the signal very often. However, we did not find references to such direct experiments in the literature~~ is most likely, $m_{14} = 0 \pm 0.05$, whereas $m_{12} = -0.22 \pm 0.2$. This means that in 30% of cases the measured depolarization and amplitude of the signal depend on the orientation of the lidar reference plane relative to the direction of the preferential orientation of the particles. In other words, when a linear polarized lidar rotates around the vertical axis, the characteristics of the backscattered signal (amplitude, depolarization) should change cyclically. However, such direct measurements are unknown to the authors~~.

It should be mentioned that ~~in~~ most of the works used 532 nm~~the polarization characteristics of the signal are measured at a~~ wavelength for measurements.~~of 532 nm.~~ Due to technical difficulties, only a small number of works use the first harmonic of the Nd: YAG laser (1064 nm) that is optimal for recording aerosol layers (~~Haarig et al., 2016; Veselovskii et al., 2017;~~ McGill et al., 2002; Burton et al., 2015; Haarig et al., 2016; Haarig et al., 2017; Veselovskii et al., 2017). The assumption of independence of crystalline particles scattering of~~by crystalline particles on~~ the wavelength is not always justified (Tao~~Borovoi~~ et al., 2008~~2014~~; Vaughan et al., 2010; ~~Borovoi~~Tao et al., ~~2014~~2008). Therefore,~~, a~~ comparison of ~~the~~ polarization and amplitude (color ratio) of signals at two wavelengths can provide the additional information about ~~the~~ properties of crystalline particles.

The optical properties of ice clouds, including their effect on the radiation balance, are determined by both the microphysical properties of crystalline particles and the presence of their orientation. These properties are in turn determined by complex meteorological processes in the clouds. Therefore, ~~The article describes a scanning polarization lidar LOSA-M3 developed at the IAO SB RAS. The first results of investigation of the crystalline particles orientation carried out with this lidar are presented. The main purpose of this lidar is~~ the study of the orientation of crystalline particles provides significant information about these processes. The article describes a scanning polarization lidar LOSA-M3, developed at the IAO SB RAS. The first results of studying the crystalline particles orientation by means of this lidar are given herein. The main purpose of this lidar is to study the optical characteristics of the mid- and high-level ice clouds~~crystal clouds of the upper and middle layers~~ at two wavelengths - 532 and 1064 nm. The design, optical scheme and principle of operation of the scanning polarization lidar are described in Sect. 2. Methods of instrument setup and calibration of the polarization channels are described in Sect. 3. Examples of observations of horizontally oriented particles in the cirrus clouds are given in Sect. 4.

2 Lidar description

Scanning polarizing lidar LOSA-M3 is a continuation of a series of small-size~~sized~~ lidars LOSA-MS and LOSA-M2, developed and operated in the IAO SB RAS (Bairashin et al., 2005, 2011) in the ~~-~~Laboratory of Optical Sensing of the Atmosphere ~~-~~(LOSA). All of these lidars are intended primarily for use in field~~expeditionary~~ conditions, which impose~~imposes~~ certain restrictions on the weight-dimensional characteristics and the energy potential of the device. The main features of LOSA-M3 lidar are the following: 1) ~~-~~automatic scanning device~~drive~~, which allows to change the direction of sensing~~sounding~~ within the upper hemisphere at the ~~a~~ speed of up to 1.5 degrees~~ degree~~ per second with the accuracy of ~~the set~~ angle measurement setting at least ~~no worse than~~ 1 arc ~~angle~~ minute; 2) ~~) the~~ separation of ~~the~~ polarization components of the received radiation ~~-,~~ $I_{\parallel}$, which coincides with the original radiation, and the component $I_{\perp}$ orthogonal to it, is carried out directly behind the receiving telescope, without installing the elements distorting ~~the~~ polarization, such as ~~-of the elements -~~dichroic mirrors and beamsplitters; and 3)~~)~~ continuous alternation ~~from impulse to impulse~~ of the initial polarization state (linear - circular) from pulse to pulse that ~~which~~ makes it possible to detect the deviations~~evaluate some elements~~ of BSPM from diagonal shape (Balin et al., 2011). A photograph~~. The appearance~~ of the lidar system is shown in ~~the~~ Fig. 1.

The optical scheme of the lidar is shown in Fig. 2. The Q-Smart 850 (Quantel) laser with a fundamental harmonic energy of 850 mJ is used with~~,~~ the repetition frequency of ~~is~~ 10 Hz (externally triggered). Radiation~~. The radiation~~ is linearly polarized, but the ~~plane of~~ polarization ~~plane~~ of the second harmonic (532 nm) is rotated by 45~~-~~° relative to the first. For coincidence of the ~~To reconcile the~~ polarization planes, the ~~a~~ phase plate *PP1* with the ~~having a~~ phase shift of 20 wavelengths for λ = 532 nm and 9.5 wavelengths for λ = 1064 nm is installed. The rotation of this plate causes the rotation of~~used. Turning the plate achieves~~ the ~~coincidence of the planes of~~ polarization plane for 1064 nm but does not affect the polarization of 532 nm. Turning the plate helps achieve the coincidence of the polarization planes for two harmonics. The Glan prism *GP* improves the polarization contrast of ~~the~~ radiation. The quarter wave λ/4 phase plate *PP2* serves to transform the polarization state (linear-circular).

Rotation~~The rotation~~ of the phase plates (the analogous plate *PP3* is placed in front of the analyzer) is performed by means of the ~~a~~ rotating platform 8RU-M (Standa) in synchronism with the ~~sending~~ laser pulses frequency. Thus, ~~each subsequent pulse~~ the phase plate can rotate by ~~be rotated at~~ 45° between pulses;~~°,~~ at the same time, the state of polarization will consistently change from linear to circular and vice versa. Lidar ~~Immediately, we note that the lidar~~ signals are separately recorded for each position of the plates *PP2* and *PP3* and can be summed up (accumulated) in ~~during~~ further processing for a certain period of time. Usually it takes~~, usually~~ from ten seconds to one ~~a~~ minute. Thus, a ~~the~~ synchronous rotation of two plates – *PP2* in the transmission channel and *PP3* in the receiver - allows measuring~~you to measure~~ the polarization characteristics (e.g. depolarization ratio~~-~~ $\delta = I_{\perp} / I_{\parallel}$) simultaneously for both linear and circular polarizations. ~~This makes it possible to exclude the variability of elements of the scattering matrix during the observation time.~~

We have two sets of quarter-wave plates. One set is designed for 532 nm, another set for 1064 nm. For the wavelength of installed plates (below are the results only for installed 1064 nm plates) we can investigate both linear and circular polarizations. For the second wavelength (532 nm) polarization state when turning 45 degrees is not determined. However, in the position where the axis of the rotating phase plate coincides with the plane of polarization of the transmitter, the radiation remains linearly polarized for any wavelength. So the measurements for the wavelength of λ = 532 nm were carried out only for linear polarization of radiation. Of course, in our lidar we can use a quarter-wave plates for 532 nm if such experiments were planned. A plate rotation algorithm is discussed more detailed below in Sect. 3.2.

The beam is collimated by the 7-fold achromatic expander *BE*, designed at the IAO SB RAS (Kochanenko et al., 2012). Two receivers are used – an achromatic lens *AL* with the 40 mm diameter and 200 mm focus for the near range, and Cassegrain mirror lens *CL* with the 200 mm diameter and 1000 mm focus for the far range. The iris diaphragms *FS1*, *FS2* in the focal plane of each lens determine the telescope field of view. A special feature of the Cassegrain lens design is installation of a video camera *VC* behind the secondary mirror, which is getting radiation through an annular diaphragm in the outer area of the secondary mirror (Simonova et al., 2015). The camera has a global shutter and is synchronized along with laser pulses. This camera setup allows observing the image of the laser spot on the objects around without parallax. It~~The beam is collimated by a 7-fold achromatic expander *BE*, developed in the IAO SB RAS (Kochanenko et al., 2012). Two receivers are used – an achromatic lens *AL* with a diameter of 40 mm and a focus of 200 mm for the near zone, and Cassegrain mirror lens *CL* with a diameter of 200 mm and a focus of 1000 mm for the far zone. Iris diaphragms *FS1*, *FS2* in the focal plane of each lens determine the field of view of telescopes. A special feature of Cassegrain lens design is the installation of the video camera *VC* behind the secondary mirror, which is emitted through an annular diaphragm in the outer area of the secondary mirror (Simonova et al., 2015). The camera has a global shutter and is synchronized by laser pulses. This camera setup allows us to observe without parallax the image of the radiation spot at the object to which the laser~~

~~radiation is directed. This~~ is especially important for setting~~tuning~~ the lidar field of view and for excluding~~to exclude~~ the possibility of lidar orientation towards residential buildings.

The signal from the receiver of the near range~~zone~~ through the optic fiber *Fb* is fed to the mirror shutter (aluminium coated obturator) *MS* , by means of which the signals of the near and far ranges~~zones~~ are alternately switched. The near range radiation is reflected from the mirror obturator, the far zone radiation passes directly with the open position of the obturator. The small receiver is closer to the transmitter, so the transition to range-square mode starts earlier (80-100 m) than for the large receiver (800-900 m). During data processing signals from near range (50-1200 m) and far range (400 m-15 km) fit together at a distance of 800-900 m when range-square mode for large receiver starts. Of course, the silica optical fiber (1 mm diameter) destroys the polarization state of the signal, so near-range data cannot be used for polarization analysis.

Shutter controller sets the obturator rotation frequency, the rotation speed of the phase plates and externally triggers the laser. So laser pulse frequency is about 10 pulse per second, but its exact value is synchronized with the rotation of the mirror obturator and platforms with phase plates.

There may be times when we are only interested in distant objects, such as high-level clouds. In this case, the obturator's rotation speed doubles, and the laser only starts when the shutter is open. The frequency of the laser pulses remains the same (10 Hz), but only far range signals are recorded.

The lens *L* forms a quasi-parallel beam that enters through the phase plate *PP3* (similar to the plate *PP2*) to the Wollaston prism *WP*. The prism divides the beam into two components with orthogonal polarization, which are further divided along the wavelengths by dichroic beamsplitters. Unlike the schemes in which the wavelength division is carried out before ~~the~~ separation of polarization components, there is no distortion of the polarization state when reflected from dichroic elements and there is no need to apply laborious calculations of the instrument vector and correction of the measured polarization (Di et al., 2016).

A~~In a beam corresponding to cross-polarization, a~~ beamsplitter *BS1* (Di-757, Semrock) is placed in the cross-polarization channel, transmitting radiation of 1064 nm and reflecting 532 nm. In the channel, corresponding to ~~the~~ initial polarization, beamsplitters *BS2* (transmitting~~transmits~~ 1064 nm) and *BS3* (reflecting~~reflects~~ 532 nm and transmitting~~transmits~~ 607 ~~-~~nm) are installed. The radiation is detected by photodetectors in the analog mode: the avalanche photodiodes *APD1*, *APD2* for 1064 nm (C30956EH-TC Perkin Elmer, 3 mm diameter of the receiving area~~ 3 mm~~), photoelectric multipliers *PM1*, *PM2* (H11506 Hamamatsu) for 532 nm. Weak signals of Raman scattering at 607 nm are recorded ~~in the photon counting mode~~ with the photomultiplier *PM3* (H11706P Hamamatsu) in the photon counting mode. Part of ~~). A part of the~~ 532-nm radiation is removed by the glass plate *BS4* on the photomultiplier *PM4* (H11706P), operating~~which operates~~ in the photon counting mode, which allows comparing the signals at 607 and 532 nm within one dynamic range. Interference filters (*IF*) with bandwidth about 1 nm are placed in front of the detectors.

The signals from ~~the~~ photodetectors are processed by 12-bit ADCs LA-n12USB (Rudnev-Shilyaev) in ~~the~~ case of analog~~current~~ signals or by a 200 MHz~~Mcps~~ photon counter (IOA SB RAS) for Raman signals and input to the computer. Peculiarity of lidar~~Lidar's feature~~ is ~~the~~ alternation of the transceiver~~transceiver's~~ parameters from pulse to pulse:

changing~~the change~~ of signals from the near and far ranges~~zones~~, the angle of ~~rotation of~~ the phase plates' rotation, and the rotation angle of the lidar during scanning.~~as a whole.~~ This eliminates a ~~the~~ possibility of accumulating signals directly after digitizing. In our case, each signal is assigned ~~A scheme has been adopted in which~~ a digital code, corresponding to the position of ~~the~~ lidar elements~~, is assigned to each signal in digital form~~ and the signals are sorted~~sorted already~~ during computer processing.

3 Tuning of lidar optical elements

3.1 Coinciding the polarization~~Polarization~~ planes

One of the main sources of errors in polarization measurements is a ~~the~~ discrepancy between the polarization planes of the emitting and receiving channels. The ~~.~~Glan prism (*GP* in Fig. 2) is installed in a rotating frame and allows aligning~~you to align~~ the planes of ~~the~~ emitter and receiver. Accuracy~~The accuracy~~ of ~~the~~ installation angle is θ=34′=0.0125 rad. Figure 3 shows the measured value of the cross-polarized component (normalized to the minimum = ~~=~~1), depending on the angle of the prism rotation~~ of the head~~. A signal from a uniform aerosol layer with a constant value of δ~1% was recorded with averaging in over 4.2-5 km range and 3 minutes interval.

Let us have the signal components $P_\parallel$ and $P_\perp$, and a ~~the~~ true depolarization ratio $\delta = P_\perp / P_\parallel$. Signal at the cross-polarization receiver, when the prism position is inaccurate, will be $P'_\perp = P_\perp \cos^2\alpha + P_\parallel \sin^2\alpha \approx P_\perp + P_\parallel \alpha^2$ (θ~~α~~ is a small setting~~an installation~~ angle error). Hence, the measured depolarization ratio will be $\delta' = P'_\perp \big/ P_\parallel = \delta + \alpha^2$, and the error of measured depolarization ratio (due to inaccurate prism position) is Δδ=θ^2~~α^2~~=0.000156≈0.016%.

3.2 Phase plates setup

Phase quarter-wave plates are mounted on a rotating platform driven by a stepper motor, working 1200 steps per revolution. One step of the platform is 0.3° and takes 0.68 ms of time, which allows the plate to rotate 45 degrees in~~during~~ the time period between two laser pulses (about 100 ms). During ~~For~~ one revolution of the platform 8 laser shots are made. Positions~~The positions~~ of the plates A (transmitter) and B (receiver) for four consecutive pulses are shown in Fig. 4~~a~~. The bold line shows the direction of a ~~the~~ fast axis of the plates. With such an arrangement of ~~the~~ axes, the signals of the cross-polarized component with both linear and circular polarization are recorded by the same photodetector.

The rotation angle setting is monitored by the zero position sensors of ~~the~~ platforms. When installing the plates in the platform frame~~, of~~ the plate ~~platform, the~~ axis ~~of the plate~~ can be shifted relative to the sensor at~~by~~ a certain angle, initially unknown. However, a laser pulse must be produced at the moment when the axis of the plates coincides with the reference plane of the lidar. The exact positions of the plates in the frame is set separately for plate A and B. We set~~Fig. 4b shows a~~

~~situation where, for plates A and B, from the instant of triggering the sensors to the laser pulse, passes 31 ms (45 steps) and 23 ms (34 steps), respectively. The situation repeats every 8 pulses.~~

~~To install the plates, a part of a homogeneous atmosphere with a small aerosol content is selected. Only~~ one plate (e.g. plate B) in its ~~is inserted into the~~ channel (receiver for plate B) and turn on the rotation. A section of a homogeneous atmosphere with small aerosol content is selected. Figure 5a shows the lidar signals from two photodetectors (P_{co} and P_{cros}), summarized over all positions of plate B (red and green lines). A height range ~~A section~~ from 6 to 9 km was chosen, on which the depolarization ratio (blue line) is constant.

For each pulse, the rotation angle of the plate was recorded and the average value of the depolarization ratio over the range of 6–9 km was calculated. These values are shown in Fig. 5b (bottom frame). The dependence averaged over 30 minutes is shown in the upper frame in Fig. 5b. ~~Fig. 5b shows the depolarization ratio for each pulse (below) and averaged over a 30 minute record (top).~~ Minimal depolarization is observed at the 34th step of the platform. The accuracy of platform setting ~~installation accuracy~~ is ± 1 step, which corresponds to 0.03% ~~an~~ error ~~of 0.03%~~ with respect to depolarization ratio. Similar adjustment of the plate A gives an exact position at the 45th platform step.

A timing diagram in Fig. 6 shows the position of the laser pulses relative to the zero position of the plates. 31 ms interval (45 steps) for plate A and 23 ms (34 steps) for plate B passes before the first laser pulse. The situation repeats every 8 pulses. As already mentioned, the frequency of laser pulses is strictly synchronized with the rotation of the plates.

The diagrams indicated in Figs. 4, 6 refer to the cases of registration only the far range signals. If we register both near and far range signals, the plates rotate through the angle 22.5° between laser pulses. Intermediate positions correspond to the near range signals and have an undefined polarization.

3.3 Calibration of the polarization channels

Measurements of the polarization of backscattered radiation require careful consideration of polarization distortions in the receiving paths and ~~the~~ sensitivity of ~~the~~ photodetectors in the channels of ~~the~~ original and cross-polarization (Freudenthaler, 2016; Belegante et al., 2018; McCullough et al., 2018~~; Freudenthaler,2016~~). The task of observations in lidar networks is to monitor the optical and microphysical properties of ~~the~~ aerosol, ~~for~~ which requires restoring~~it is necessary to restore~~ not only the backscattering coefficient, but also the lidar ratio and attenuation. Therefore, a large number of lidars are designed~~created~~ as aerosol-Raman (Althausen et al., 2000; Whiteman et al., 2007; Reichardt et al., 2012; Groß et al., 2015; Haarig et al., 2017; Madonna et al., 2018~~; Whiteman et al., 2007; Groß et al., 2015~~) or multiwave high spectral resolution ~~(HSRL)~~ lidars (HSRL) (Eloranta, 2005; Burton et al., 2015~~; Haarig et al., 2017; Althausen et al., 2000; Eloranta, 2005~~). Most of these lidars use dichroic beamsplitters as wavelength dividers, and polarizing elements (film polarizers) are installed after the beam~~beam~~ splitters and deflecting mirrors (Nott~~McCullough~~ et al., 2012~~2018~~; Engelmann et al., 2016; ~~McCullough~~Nott et al., ~~2018~~2012). This leads to distortions in recording~~the registration~~ of polarization components, which require complex procedures for determining the eigenvectors of polarization of the lidar and taking them into account when restoring the polarization state of ~~the~~ scattered radiation (Alvarez et al., 2006; Haymann et al., 2012; ~~Di et al., 2016;~~ Freudenthaler~~, 2016; Freudenthaler~~ et al., 2009; Bravo-Aranda et al., 2016; Di~~Alvares~~ et al., ~~2016; Freudenthaler, 2016~~2006).

Measurements of ~~the~~ polarization characteristics of backscattered radiation simultaneously for several wavelengths were carried out by different groups: 347+697 nm (Pal and Carswell, 1978), 355+532 nm (~~Groß et al., 2015;~~ Althausen et al., 2000; ~~Engelmann et al., 2016;~~ Summa et al., 2013; Groß et al., 2015; Engelmann et al., 2016), and 355+532+1064 nm (~~Haarig et al., 2016;~~ Burton et al., 2015; Haarig et al., 2017; Hu et al, 2019). The~~). Lidar~~ LOSA-M3 lidar measures polarization components at wavelengths of 532 and 1064 nm. At the same time, the polarization components are separated~~distinguished~~ directly behind the receiving telescope, before the radiation is separated according to~~by~~ wavelength. This ~~In this~~ scheme has ~~, there are~~ no distortions of the polarization state ~~upon reflection~~ from dichroic mirrors reflection; therefore, there is no need to use laborious calculations for~~of~~ the instrumental vector of the transmitting-receiving channel and correction of~~correcting~~ the measured polarization. In this case, ~~to measure the magnitude of the depolarization ratio,~~ it is sufficient to determine the relative sensitivity of ~~the~~ detectors in both lidar channels ~~to measure the magnitude~~ of the depolarization ratio. The channel calibration problem is solved in most devices for polarization measurements. An exception is devices where signals ~~lidar. If we ignore the devices that used a sequential change~~ of different polarization are sequentially directed to ~~polarizations on~~ one photodetector (Platt, 1977; Eloranta and Piironen, 1994; McCullough et al., 2017)~~), this problem was solved in all devices for polarization sounding~~.

The relative sensitivity of photodetectors can be determined by observing the ~~a~~ source with ~~a~~ known polarization — it ~~this~~ can be a non-polarized source (Sassen and Benson, 2001), or an atmospheric layer with purely molecular scattering (Biele et al., 2000~~Noel and Sassen, 2005~~; Noel et al., 2002; Volkov et al., 2002; Kaul et al., 2004; Noel and Sassen, 2005~~2004; Biele et al., 2000; Volkov et al., 2002~~). However, the depolarization ratio for ~~in~~ molecular scattering depends significantly ~~depends~~ on the bandwidth of ~~the used~~ interference filter used, since rotational Raman lines can contribute to the signal (~~She, 2001;~~ Young, 1980; She, 2001). For pure Rayleigh scattering, the depolarization ratio is δ=0.00365, with a wide filter, δ=0.015. It ~~This~~ leads to an ambiguous lidar calibration.

The most common calibration is associated with ~~the~~ rotation of the separation plane for~~of the~~ polarization components ~~component~~ by 90° (Freudenthaler, 2016). In this case, the photodetectors change places with respect to the polarization components. Turning~~of polarization. Rotation~~ by 90° can be carried out physically ~~–~~by rotating the entire photodetector unit (Yoshida et al., 2010; Strawbridge, 2013), or by rotating the half-wave phase plate, which can be installed both in the transmitter channel (Spinhirne et al., 1982) ~~-~~and the receiver (McGill et al., 2002; Reichardt et al., 2012). In ~~the~~ previous lidars of the LOSA series (Balin et al., 2009), ~~a~~ mechanical rotation of the photodetector unit by 90° was used. The intensity ratios in both channels were taken into account and ~~, which~~ made it possible to eliminate possible changes in the object brightness ~~of the object~~ during turning.~~the turn.~~ When calibrating with this method, you can choose any stable aerosol-cloud formation as a scattering object, which is characterized by a noticeable (>10%) and constant depolarization ratio during the measurement period.

To measure the depolarization ratio of ~~the~~ backscattered radiation, the relative sensitivity of detectors must be known. Thus, in ~~In~~ our lidar we offer a new method for a ~~of~~ continuous rotation of λ/2 phase plate, temporarily installed in the receiver module instead of λ/4 plate *PP3* in Fig. 2. For the light backscattering phase matrix (BSPM), we take a 4×4 matrix **M** relating the Stokes vectors of radiation scattered in the direction toward the source $\mathbf{S}=\left[I,Q,U,V\right]^T$ with the Stokes vector $\mathbf{S_0}$ of radiation, incident on an ensemble of particles. Polarization components are expressed as $I_{\parallel}=\left(I+Q\right)/2,\ I_{\perp}=\left(I-Q\right)/2$.~~–~~ Let us assume that laser radiation is linearly polarized (the initial vector is $\mathbf{S}_0^L=\left[1,1,0,0\right]^T$). Then the scattered Stokes vector is $\mathbf{S}=\mathbf{MS}_0^L=\left[m_{11}+m_{12},m_{12}+m_{22},-m_{13}-m_{23},m_{14}+m_{24}\right]^T$. If we install ~~set~~ the λ/2 phase plate ~~before the polarization prism~~ with matrix $\mathbf{L}=\begin{pmatrix}1 & 0 & 0 & 0\\ 0 & \cos 4\varphi & \sin 4\varphi & 0\\ 0 & \sin 4\varphi & -\cos 4\varphi & 0\\ 0 & 0 & 0 & 0\end{pmatrix}$ before the polarization prism in the receiver, where~~,~~ φ is the rotation angle, the Stokes vector will be

$$\mathbf{S}=\mathbf{LMS}_0^L=\begin{pmatrix}m_{11}+m_{12}\\ (m_{12}+m_{22})C_4-(m_{13}+m_{23})S_4\\ (m_{12}+m_{22})S_4+(m_{13}+m_{23})C_4\\ m_{14}+m_{24}\end{pmatrix}$$

, where $C_4=\cos 4\varphi,\ S_4=\sin 4\varphi$. Polarization components $I_{\parallel}, I_{\perp}$ are~~is~~ different~~:~~ $2I_{\perp}^{\parallel}=m_{11}+m_{12}\pm(m_{12}+m_{22})C_4\mp(m_{13}+m_{23})S_4$ (the upper sign is for $I_{\parallel}$, the lower for $I_{\perp}$). However,~~But~~ the integral for a complete turn of the plate over the angle φ~~:~~ $\int\limits_{2\pi} I_{\parallel,\perp}d\varphi=\pi\left(m_{11}+m_{12}\right)$ is the same for each polarization component, regardless of the values of matrix elements. The ratio of ~~the~~ measured values of the integral for two components $K=\int I_{\perp}d\varphi/\int I_{\parallel}d\varphi$ gives us the value of ~~the~~ relative sensitivity of the polarization channels.

Calibration procedure is done ~~made~~ separately for 532 and 1064 nm. The method works for any initial state of polarization and for any BSPM of aerosol layer. Unlike the Δ90 method, there is no need to ensure extremely accurate setting of the plate rotation angle, but during the ~~turn of the~~ plate turning (about 20 seconds), ~~the~~ change in the scattering properties of the object should be minimal. Fig. 7 shows~~6 depicts~~ one of ~~the~~ calibration records made ~~held~~ on 07 May ~~.05.~~2017, demonstrating the errors of the applied method. The upper~~Upper~~ part (7a~~6a~~) shows the record of a ~~the~~ signal (1064 nm) integrated by the plate rotation angle~~ of the plate~~, components $I_{\parallel}$ (green) and $I_{\perp}$ (red~~blue~~). Integration was carried out during four ~~for 4~~ revolutions of the plate. Fig. 7b shows~~6b depicts~~ the value of calibration constant *K,* calculated in the ~~1800-~~

~~8000 m~~ height range of 1800-8000 m. In this case, the mean value K=1.91. Similar calibration procedures were carried out before each measurement in April and June 2018. All values K did not deviate by more than ±0.05.

4 Observations of ice~~crystalline~~ clouds during lidar zenith scanning

In this paper~~,~~ we present the results of observations of the ice~~crystalline~~ cloud cover under the lidar zenith scanning. Measurements were made in Tomsk (56°28'N, 85°E) in April-June 2018. Scanning was carried out at the ~~a~~ rate of 0.5 degrees per second, which corresponds to three arc minutes ~~a~~ shift of sensing ~~in the~~ direction ~~of sounding by 3 minutes~~ between laser pulses. The angle is measured from the vertical position of ~~the~~ radiation beam, which was set ~~established~~ with an error of ± 5 arc minutes. Moreover, in some cases~~,~~ the scanning was carried out with the lidar axis passing through the zenith (ranging from -1 ° to +~~4~~ °), which made it possible to control the accuracy of the lidar vertical setting. The measurement data array is not large and is mainly used here for testing the lidar performance.

4.1 Zenith scanning at 1064 nm wavelength

Below we present the data for polarized components at 1064 nm related to radiation with initial circular polarization. The depolarization of linearly polarized radiation is generally less than that of circularly polarized radiation. For randomly distributed particles, the linear depolarization is two times less than for circular (Mishchenko and Hovenier, 1995; Gimmestad, 2008). For oriented particles the difference is smaller, since the BSPM element ~~Figure 7 shows the sounding data on April 6, 2018, 10:25 local time. 7a depicts the component~~ $I_{\parallel}$ is not equal to zero (Balin et al., 2011). Low value of depolarization results in that the cross-polarized component ~~(signal intensity, mV), 7b depicts the depolarization ratio~~ $\delta^{Circ} = I_{\perp}/I_{\parallel}$ very often does not stand out against the background of the photodetector noise in the specular reflection. Therefore, the dependences of polarized components for 1064 nm are presented for initial circular polarization of laser beam. Dependences ~~(%), measured for the circle initial polarization of the laser beam, 7c - the zenith scanning angle (minutes). Date of weather sounding (7d) are taken from the site of the Universty of Wyoming (http://weather.uwyo.edu).~~

~~The duration of the recording is 300 seconds. In the interval from 120 to 250 seconds, scanning was carried out in the range from 0 to 2 degrees. The behavior of the two cloud layers is clearly different. The characteristics of the upper layer (8-10 km) do not change when scanning, which indicates the chaotic orientation of the particles in the cloud. In the lower layer (6.5-7 km), a pronounced modulation is observed, characteristic for a predominantly horizontal orientation of the particles. The maximum intensity of the signal with the vertical sounding direction corresponds to a minimum of the depolarization ratio. The extremely low value~~ δ^{Circ} for linear and circular polarizations for scan angles 0-4° do not differ within the error limits.

Figure 8 shows the lidar data observed on 6 April 2018. The recording starts at 10:25 local time (UTC+7), time from the start is shown on X-axis. Fig. 8a gives the component ~~in the zenith direction~~ $\delta_{Zen}^{Circ} \approx 4-5\%$ (signal intensity, mV); 8b – the depolarization ratio $\delta^{Circ} = I_{cros}^{Circ} / I_{co}^{Circ}$, %; 8d – the zenith scanning angle (arc minutes), time axis is aligned with Fig. 8a and 8b. Data of weather sounding (8c) are taken from the site of the University of Wyoming (http://weather.uwyo.edu). Radiozonde sounding was carried out at Novosibirsk station, about 250 km from Tomsk to SW, two records were made at 07:00 and 19:00 LST. Of course, due to the distant location of the station and the rare launches of probes (once every twelve hours) these data do not describe the fine structure of the ice cloud.

Duration of recording is 300 seconds. In the interval from 120 to 250 seconds, scanning was carried out in the range from 0 to 2 degrees. A high-level cloud consists of two layers. The thin bottom layer (6600-7000 m) has a temperature minus 26-31°C, the top layer (7800-9800 m) temperature is 37-52°C below zero. The behavior of these layers is significantly different. Characteristics of the top layer do not change when scanning, which indicates the chaotic orientation of particles in the cloud. In the bottom layer a pronounced modulation of signal intensity and polarization is observed, characteristic for a predominantly horizontal orientation of particles. The maximum intensity of signal with the vertical sensing direction corresponds to the minimum of depolarization ratio. An extremely low value δ^{Circ} in the zenith direction $\delta_{Zen}^{Circ} \approx 4-5\%$ corresponds to the specular reflection.

The other situation is observed on 2 June 2018, 09:55 LST (Fig. 9). Duration of this recording is 550 seconds. The maximum inclination was 4°, the beam passed through the vertical by 1° while scanning. In Fig. 8a we saw clearly expressed single line of maximum signal, because the vertical position was the edge position when scanning. When we scan our lidar from 4° to -1° and back, vertical positions (0°) are close to each other. So in Fig. 9a two lines of maximum signals are close to each other and look like a double line.

~~corresponds to the specular reflection.~~

~~Another situation is observed on June 02, 09:55 LST (Fig. 8). The duration of this recording is 550 seconds. The maximum slope was 4°, while scanning the beam passed through the vertical by 1° (this leads to the appearance of double lines of maximum intensity in Fig.8a). A cirrus cloud with a complex structure occupies the layer 8 - 11.7 km.~~ A cirrus cloud with a complex structure extends in a layer of 8 - 11.7 km. The temperature in the cloud varies from -34°C to -60°C. Pronounced ~~pronounced~~ modulation of the signal intensity and depolarization ratio are~~is~~ observed throughout the entire height of the cloud. As in the previous case, the maximum intensity of the signal corresponds to the ~~a~~ minimum of depolarization ratio. However, the minimum values δ_{Zen}^{Circ} differ~~are~~ significantly ~~different~~ in various~~different~~ parts of the cloud. In the lower part of the cloud, the value~~s~~ $\delta_{Zen}^{Circ} \approx 0.6$ ~~, which~~ indicates the predominance of chaotically oriented particles and a small proportion of horizontally oriented particles. In the upper part (11.2-11.7 km) $\delta_{Zen}^{Circ} < 5\%$ ~~. This~~ is characteristic of mirror reflection and indicates a pronounced horizontal orientation of particles in this part of the cloud.

Values δ^{Circ} ~~The values~~ outside the vertical are close to 100% throughout the entire cloud thickness ~~of the cloud~~. This suggests that particles in the cloud differ only in the degree of their horizontal orientation.

4.2 Dependence of the signal intensity on the lidar tilt angle

The ice clouds ~~of the upper layers~~ never constitute a formation uniform in height and constant in time. Pronounced ~~In the structure of crystalline clouds, pronounced~~ layers with the ~~a~~ thickness of ~~the order of~~ hundreds of meters are regularly observed in the structure of ice clouds. They differ in the state of depolarization and signal intensity from the higher and lower regions and are supposedly homogeneous in composition and degree of particle orientation. However, the signal intensity and the ~~value of the~~ depolarization ratio do not remain constant, but vary with time rather quickly ~~change with time~~. The height of ~~the~~ layers also varies.~~changes.~~ Weak values of the backscatter signals lead to the need of ~~for~~ averaging the signals over the height of the selected layer and over time about ~~of the order of~~ 3-5 minutes. As a result, ~~to measure the dependence of the characteristics of the echo signal on the angle of inclination,~~ it is necessary to pre-~~first~~ select sections of the cloud, characterized by an approximately constant value of ~~the~~ intensity and depolarization ratio, and lasting for several scan cycles to measure the dependence of echo signal characteristics on the tilt angle. An example of such ~~a~~ procedure for selecting the ~~studied~~ cloud sections to be studied is shown in Fig. 10~~9~~.

In the given 5-minute recording, 6 sections were selected (marked with rectangles) with the~~a~~ duration from ~~of~~ three to seven scan cycles. The rest of ~~remaining~~ cloud portions ~~on this record~~ were not analyzed on this record. In total, about 20 records were selected during observations on 2 ~~the observation on~~ June ~~2, 2018 and October 1,~~ 2018, ~~in~~ which have ~~there is~~ a pronounced dependence on the tilt angle, ~~of the lidar~~ and there is no signal overflow when the lidar is oriented to zenith. ~~The following are typical examples of the dependences of the intensity of the polarization components on the angle of inclination.~~

Figure 11~~10~~ indicates the typical dependences~~dependencies~~ of signal intensities of parallel $I_{\parallel}^{circ}$ (circular initial polarization) and cross-polarized I_{cros}^{circ} $\cancel{I_{\perp}^{circ}}$ components on the tilt angle α. The record shown in Fig. 11a~~10a~~ was registered at 12:00 LST with averaging of ~~the~~ characteristics over the layer from 11470m to 11600m. The record shown in Fig. 11b~~10b~~ was made at 10:00 LST with averaging of ~~the~~ characteristics over the layer from 10980 to 11270m. The signal was accumulated during 10 minutes. These ~~obtained in~~ measurements and all data, obtained in June ~~and October~~ 2018, are ~~are well~~ described satisfactorily by the following exponential dependence~~distribution~~

$$I(\alpha) = I_0 + A\exp(-|\alpha - \alpha_0|/w) \qquad (1)$$

(red line in Fig. 11~~10~~), where I is the signal intensity, I_0 is the offset of dependence determined by a signal ~~intensity~~ without the specular component ~~(α>>4°)~~, A is the ~~a~~ constant, depending on the contribution of specular reflection in ~~the~~ total intensity, α is the tilt~~an inclination~~ angle, w determines the width of ~~the~~ distribution, and α_0 indicates the error of ~~the~~ lidar targeting to the vertical. For Fig. 11a~~10a~~ w=42 arc~~angle~~ minutes, for Fig. 11b~~10b~~ w=82′. The Gaussian function used in Noel and Sassen, 2005 ~~Ref. 11~~ (blue line in Fig. 1 is noticeably wider and~~10)~~ poorly describes the observed distribution, perhaps because it does not take into consideration the intensity~~. The main difference is determined by the underestimation of the sharp~~ peak at α=0°.

Cross-polarized signals ~~The values~~ $I_\perp$ have random variations from pulse to pulse comparable with the average value. In most cases the values of ~~in most cases shows a weak decline with the angle, but its change are smaller than the measurement errors. We can conclude that~~ $I_\perp$ show a weak decline of intensity with the angle, but these variations do not exceed instrumental errors (about 1% for depolarization ratio). ~~is practically independent on the inclination angle.~~

Figure 11a shows the variations even less the 0.5%. Moreover, a slightly noticeable maximum at α=0° looks like signal penetration from parallel to perpendicular channel. Therefore we think, that linear trend is not statistically reliable. We can conclude that I_{cros}^{circ} is practically independent on the tilt angle.

Figure 12 gives~~11 depicts~~ some selected dependences~~dependencies~~ of intensity angle distributions for component~~-~~ $I_\parallel$. We did not find any correlation of the distribution parameters (A, I_0, w) with the height of the selected area inside the cloud. So the selection of cloud portions presented in Fig. 12 is rather subjective. The only requirement is: these portions must have a pronounced dependence on the tilt angle, and there is no signal overflow when the lidar is oriented to zenith. The dependences are normalized to the value I_0 obtained by fitting according to the Eq. (1). Squares indicate the tilt angles, corresponding to the distribution width w. For all measurements the value w is within 40-160 arc~~150 angle~~ minutes. The shift α_0 of the curve maximum from 0° is less than 2 minutes, which indicates a good lidar orientation ~~of the lidar~~ to the zenith. Since the signal intensity offset I_0 ~~for α>>4°~~ is determined by ~~all~~ particles with any orientation (both random and horizontal), the ratio $I_\parallel(0°)/I_0$ may reflect ~~shows~~ the contribution~~proportion~~ of mirror~~horizontally oriented~~ particles to~~in~~ the lidar signal. The left frame shows cases~~total mass~~ of ~~crystals in~~ a fairly narrow distribution, w is within 40-75 arc minutes. The ratio $I_{co}^{Circ}(4°)/I_0$ is less then 1.1. The right frame shows cases with $I_{co}^{Circ}(4°)/I_0 > 1.1$, among these cases there are distributions with a large (up to 159 arc min) width~~given section of the cloud~~.

~~Previous data related to radiation with initially circular polarization. The degree of depolarization of linearly polarized radiation is generally less than that of circularly polarized radiation. For chaotically oriented particles, the depolarization is less than half (Mishchenko and Hovenier, 1995; Gimmestad, 2008), for oriented particles the difference is smaller, since the BSPM element~~ $\cancel{m_{12}}$ ~~is not equal to zero (Balin et al., 2011). The low value of depolarization leads to the fact that in specular reflection the cross-polarized component~~ $\cancel{I_\perp^{Lin}}$ ~~very often does not stand out against the background of the noise of the photodetector. Therefore, the dependences~~ $\cancel{I_\perp(\alpha)}$ ~~were investigated for circular polarization. The dependences~~ $\cancel{I_\parallel(\alpha)}$ ~~for linear and circular polarizations for scan angles 0–4° do not differ within the error limits.~~

4.3 Angular distributions for green and infrared wavelengths

The obtained~~resulting~~ dependence $I_{\parallel}(\alpha)$ in general terms should correspond to ~~the~~ distribution of specularly reflecting particles along the angles of deviation from the horizontal plane (flutter). However, due to the phenomenon of ~~diffraction of~~ backscattered radiation diffraction on the particle's contour (Borovoi et al., 2008), the distribution is wider than the distribution of particles along the ~~tilt~~ angles of inclination. In addition, the ratio of backscattering coefficients (color ratio) for α >> 4° (and for randomly oriented particles in any direction) is not equal to unity (Tao~~(Borovoi~~ et al., 2008~~2014~~; Vaughan et al., 2010; ~~Borovoi~~Tao et al., ~~2014~~2008). Therefore, the distribution $I_{\parallel}(\alpha)$ may depend on the radiation wavelength.

As mentioned in the Sect. 2 the~~In our lidar,~~ measurements for the ~~a~~ wavelength of λ = 532 nm were ~~are~~ carried out only for linear polarization of radiation, as we used ~~since~~ the quarter-wave plates in the transceiver for the wavelength~~are made for a wavelength of~~ λ = 1064 nm. ~~However, in the position where the axis of the rotating phase plate coincides with the plane of polarization of the emitter, the radiation remains linearly polarized for any wavelength. These pulses are used for measurements at a wavelength of 532 nm.~~

Two cases with the maximum angular differences are shown in Fig. 13.~~12.~~ The relative sensitivity of photodetectors at 532 and 1064 nm was not calibrated. Therefore the intensities of polarization components for 532 nm (both I_{co}^{Lin} and I_{cros}^{Lin}) were normalized so that the intensity maximum of I_{co}^{Lin} (0°) in the vertical position coincided with I_{co}^{Lin} (0°) for 1064 nm.~~, therefore, the amplitudes of the signals are shown to be the same.~~ In the left figure~~frame~~ the angle distributions are the same, in the right figure~~frame~~ the distribution for 532 nm is much wider ($I_{532}(4°)/I_{1064}(4°)=1.5$). In all other cases we have intermediate states: the distribution width *w* for 532 nm is equal or bigger than~~more then~~ for 1064 nm. The reason for such~~this~~ behavior of dependences~~dependencies~~ is not yet clear for the authors~~of the article~~.

5 Conclusions

Scanning polarizing lidar LOSA-M3 is developed and operated in the ~~IAO SB RAS in the~~ Laboratory of Optical Sensing of the Atmosphere (LOSA) at the IAO SB RAS.~~).~~ The main purpose of this lidar is to ~~the~~ study ~~of~~ the optical characteristics of the mid- and high-level ice~~crystal~~ clouds ~~of the upper and middle layers~~ at two wavelengths - 532 and 1064 nm. Lidar allows a smooth~~you to smoothly~~ change of the tilt angle ~~of inclination~~ from the vertical with simultaneous conical (azimuthal) scanning. Such ~~a~~ measurement scheme makes it possible to study ~~in detail~~ the preferential orientation of ice crystals in the clouds in detail. The lidar simultaneously measures the polarization characteristics of signals for linear and circular initial polarizations, which allows obtaining~~to obtain~~ additional information about the anisotropy of scattering particles. Since the circular polarization signal does not depend on the rotation of the lidar relative to the direction of particle orientation, this polarization can be used as a reference for investigation~~, including exploring~~ the azimuthal orientation of the particles. At the same time, the ~~a~~ lidar, like all of the LOSA ~~series~~ aerosol-Raman lidars, has a Raman scattering channel (607 nm band, for night observations) and a system for combining near and far ranges~~zones~~, which allows it to be used for observing~~to observe~~ aerosol fields in the troposphere distances of 50~~50~~ m - 15~~15~~ km.

During 2018, several series of measurements of the structure of the ice~~crystalline~~ clouds ~~of the upper layers~~ in the zenith scan mode were carried out. The results show that the contribution of horizontally oriented particles, giving a specular reflection, can vary significantly in different parts of the cloud. The dependence of ~~the~~ signal intensity on the tilt angle ~~of inclination~~ reflects the distribution of the ~~particles~~ deviation ~~of particles~~ relative to the horizontal plane, and is well described by the~~an~~ exponential dependence. Cross-polarized component $I_{\perp}$ in most cases shows a weak decline with the angle, but its variations~~change~~ are smaller than the measurement errors. We can conclude that $I_{\perp}$ is practically independent on the tilt~~inclination~~ angle. The angle distribution of ~~for~~ the radiation for 532 nm in all experiments is equal or wider than~~then~~ for 1064 nm. The reason for such ~~this~~ behavior of dependences~~dependencies~~ is not yet clear for the authors~~of the article~~.

Author contributions. GK~~GP~~ and IP designed the lidar, MN and MK developed the software, GK~~GP~~, YuB, and SN carried out the lidar measurements, SN and SS carried out the data analysis, GK prepared the manuscript with contributions from all co-authors.

Competing interests. The authors declare that they have no conflict of interest.

Acknowledgements. The authors are grateful to Anatoli Borovoi~~The reported study was funded by RFBR~~ and Alexander Konoshonkin for the fruitful discussion during the preparation of the article. The reported study was funded by RFBR,~~Tomsk region~~ according to the Research Project No. 18-55- 81001~~research project № 19-48- 700014~~ and by Project No.~~project №~~ AAAA-A17-117021310142-5.

References

Althausen, D., Müller, D., Ansmann, A., Wandinger, U., Hube, H., Clauder, E., and Zörner, S.: Scanning sixwavelength eleven channel aerosol lidar, J. Atmos. Ocean. Tech., 17, 1469–1482, 2000.

Alvarez~~Alvares~~, J. M., Vaughan, M. A., Hostetler, C. A., Hunt, W. H., and Winker, D. M.: Calibration Technique for polarization-sensitive lidars, J. Atm.Ocean Technology, 23, 683-699, 2006.

Bairashin, G. S., Balin, Yu. S., Ershov, A. D., Kokhanenko, G. P., and Penner, I. E.: Lidar LOZA-MS for investigation of aerosol fields in troposphere, Optical Engineering, 44(7), 071209-1-071209-7, 2005.

Bairashin, G. S., Balin, Yu. S., Klemasheva, M. G., Kokhanenko, G. P., Penner, I. E., and Samoilova, S. V., Aerosol-Raman lidar LOSA-M2, Quantum electronics, 41(10), 945-949, 2011.

Balin, Yu., Kaul, B., Kokhanenko, G., and Winker, D.: Application of circularly polarized laser radiation for sensing of crystal clouds, Opt. Express, 17, 6849-6859, 2009.

Balin, Yu. S., Kaul, B. V., Kokhanenko, G. P., and Penner, I. E.: Observations of specular reflective particles and layers in crystal clouds, Opt. Express, 19, 6209-6214, 2011.

Belegante, L., Bravo-Aranda, J. A., Freudenthaler, V., Nicolae, D., Nemuc, A., Ene, D., Alados-Arboledas, L., Amodeo, A., Pappalardo, G., D'Amico, G., Amato, F., Engelmann, R., Baars, H., Wandinger, U., Papayannis, A., Kokkalis, P., and Pereira, S. N.: Experimental techniques for the calibration of lidar depolarization channels in EARLINET, Atmos. Meas. Tech., 11, 1119–1141, 2018.

Biele, J., Beyerle, G., and Baumgarten, G.: Polarization lidar: Corrections of instrumental effects, Opt. Express, **7,** 427–435, 2000.

Borovoi, A., Grishin, I., Naats, E., and Oppel, U., "Backscattering peak of hexagonal ice columns and plates," Opt. Lett., 25(18), 1388–1390 (2000).

Borovoi, A., Galileiskii, V., Morozov, A., and Cohen, A.: Detection of ice crystal particles preferably oriented in the atmosphere by use of the specular component of scattered light, Opt. Express, 16(11), 7625-7633, 2008.

Borovoi, A., Balin, Yu., Kokhanenko, G., Penner, I.; Konoshonkin, A., and Kustova, N.: Layers of quasi-horizontally oriented ice crystals in cirrus clouds observed by a two-wavelength polarization lidar, Opt. Express, 22, 24566-24573, 2014.

Bravo-Aranda, J. A., Belegante, L., Freudenthaler, V., Alados-Arboledas, L., Nicolae, D., Granados-Muñoz, M. J., Guerrero-Rascado, J. L., Amodeo, A., D'Amico, G., Engelmann, R., Pappalardo, G., Kokkalis, P., Mamouri, R., Papayannis, A., Navas-Guzmán, F., José Olmo, F., Wandinger, U., Amato, F., and Haeffelin, M.: Assessment of lidar depolarization uncertainty by means of a polarimetric lidar simulator, Atmos. Meas. Tech., 9, 4935–4953, 2016.

Breon, F.-M. and Dubrulle, B.: Horizontally oriented plates in clouds, J. Atmos. Sci., 61, 2888–2898, 2004.

Burton~~Buton~~, S. P., Hair, J. W., Kahnert, M., Ferrare, R. A., Hostetler, C. A., Cook, A. L., Harper, D. B., Berkoff, T. A., Seaman, S. T., Collins, J. E., Fenn, M. A., and Rogers, R. R.: Observations of the spectral dependence of linear particle depolarization ratio of aerosols using NASA Langley airborne High Spectral resolution Lidar, Atmos. Chem. Phys., 15, 13453–13473, 2015.

Campbell, J. R., Vaughan, M. A., Oo, M., Holz, R. E., Lewis, J. R., and Welton, E. J.: Distinguishing cirrus cloud presence in autonomous lidar measurements, Atmos. Meas. Tech., 8, 435–449, 2015.

Chen, W. N., Chiang, C. W., and Nee, J. B.: Lidar ratio and depolarization ratio for cirrus clouds, Appl. Opt., 41(30), 6470–6476, 2002.

Chepfer, H., Brogniez, G., Goloub, P., Breon, F. M., and Flamant, P. H.: Observations of horizontally oriented ice crystals in cirrus clouds with POLDER-1/ADEOS-1, J. Quant. Spectrosc. Radiat. Transfer, 63, 521–543, 1999.

Cho, H. M., Yang, P., Kattawar, G. W., Nasiri, S. L., Hu, Y., Minnis, P., Trepte, C., and Winker, D.: Depolarization ratio and attenuated backscatter for nine cloud types: analyses based on collocated CALIPSO lidar and MODIS measurements, Opt. Express, 16(6), 3931–3948, 2008.

Del Guasta, M., Vallar, E., Riviere, O., Castagnoli, F., Venturi, V., and Morandi, M.: Use of polarimetric lidar for the study of oriented ice plates in clouds, Appl. Opt., 45(20), 4878–4887, 2006.

Di, H. G., Hua, H. B., Cui, Y., Hua, D. X., Li, B., and Song, Y. H.: Correction technology of a polarization lidar with a complex optical system, J. Optical Soc. Amer. A., 33(8), 1488-1494, 2016.

Eloranta, E.: High Spectral Resolution Lidar, in: Lidar: range-resolved optical remote sensing of the atmosphere, edited by C. Weitkamp, Springer, NewYork, 2005.

Eloranta, E. W. and Piironen, P.: Depolarization measurements with the high spectral resolution lidar, Abstracts 17th Int. Laser Radar Conf., Sendai, Japan, 127–128, 1994.

Engelmann, R., Kanitz, T., Baars, H., Heese, B., Althausen, D., Skupin, A., Wandinger, U., Komppula, M., Stachlewska, I. S., Amiridis, V., Marinou, E., Mattis, I., Linné, H., and Ansmann, A.: The automated multiwavelength Raman polarization and water-vapor lidar **PollyXT**: the neXT generation, Atmos. Meas. Tech., 9, 1767–1784, 2016.

Freudenthaler, V.: About the effects of polarising optics on lidar signals and the Δ90-calibration, Atmos. Meas. Tech., 90, 4181-4255, 2016.

Freudenthaler, V., Esselborn, M., Wiegner, M., Heese, B., Tesche, M., Ansmann, A., Müller, D., Althausen, D., Wirth, M., Fix, A., Ehret, G., Knippertz, P., Toledano, C., Gasteiger, J., Garhammer, M., and Seefeldner, M.: Depolarization ratio profiling at several wavelengths in pure Saharan dust during SAMUM 2006, Tellus B, 61, 165–179, 2009.

Gimmestad, G. G.: Reexamination of depolarization in lidar measurements, Appl. Opt., 47, 3795-3802, 2008.

Groß, S., Freudenthaler, V., Schepanski, K., Toledano, C., Schäfler, A., Ansmann, A., and Weinzierl, B.: Optical properties of long-range transported Saharan dust over Barbados as measured by dual-wavelength depolarization Raman lidar measurements, Atmos. Chem. Phys., 15, 11067–11080, 2015.

Haarig, M., Engelmann, R., Ansmann, A., Veselovskii, I., Whiteman, D. N., and Althausen, D.: 1064nm rotational Raman lidar for particle extinction and lidar-ratio profiling: cirrus case study, Atmos. Meas. Tech., 9, 4269–4278, 2016.

Haarig, M., Ansmann, A., Althausen, D., Klepel, A., Groß, S., Freudenthaler, V., Toledano, C., Mamouri, R.-E., Farrell, D. A., Prescod, D. A., Marinou, E., Burton, S. P., Gasteiger, J., Engelmann, R., and Baars, H.: Triple-wavelength depolarizationration profiling of Saharan dust over Barbados during SALTRACE in 2013 and 2014, Atmos. Chem. Phys., 17, 10767–10794, 2017.

Hayman, M., Spuler, S., Morley, B., and VanAndel, J.: Polarization lidar operation for measuring backscatter phase matrices of oriented scatterers, Opt. Express, 20(28), 29553-29567, 2012.

Hayman, M., Spuler, S., and Morley, B.: Polarization lidar observations of backscatter phase matrices from oriented ice crystals and rain, Opt. Express, 22(14), 16976-16990, 2014.

Hoareau, C., Keckhut, P., Moel, V., Chepfer, H., and Baray, J.-L.: A decadal cirrus clouds climatology from ground-based and spaceborne lidars above the south of France (43.9°N-5.7°E), Atmos. Chem. Phys., 13, 6951-6963, 2013.

Hu, Q., Goloub, Ph., Veselovskii, I., Bravo-Aranda, J.-A., Popovici, I. E., Podvin, Th., Haeffelin, M., Lopatin, A., Dubovik, O., Pietras, Ch., Huang, X., Torres, B., and Chen, Ch.: Long-range-transported Canadian smoke plumes in the lower stratosphere over northern France, Atmos. Chem. Phys, 19, 1173-1193, 2019.

Hunt, W. H., Winker, D. M., Vaughan, M. A., Powell, K. A., Lucker, P. L., and Weimer, C.: CALIPSO lidar description and performance assessment, J. Atmos. Ocean. Technol., 26(7), 1214–1228, 2009.

Kaul, B. V.: Symmetry of light backscattering matrices related to orientation of nonspherical aerosol particles, Atmos. Oceanic Opt., 13, 829–833, 2000.

Kaul, B. V. and Samokhvalov, I. V.: Orientation of particles in *Ci* crystal clouds. Part 1. Orientation at gravitational sedimentation, Atmos. Oceanic Opt., 18, 866–870, 2005.

Kaul, B.V., Samokhvalov, I.V., and Volkov, S.N.: Investigating of particle orientation in cirrus clouds by measuring backscattering phase matrices with lidar, Appl. Opt., 43, 6620 –6628, 2004.

Klotzsche, S. and Macke, A.: Influence of crystal tilt on solar irradiance of cirrus clouds, Appl. Opt., 45(5), 1034-1040, 2006.

Kochanenko, G. P., Simonova, G. V., Makogon, M. M., Ponomarev, Yu. N., and Rynkov, O. A., Designing a beam expander for dual-wave laser fluorescence lidar, J. Opt. Technol., 79, 217-219, 2012.

Kokhanenko, G.P., Balin Yu.S., Borovoi A.G., Klemasheva M.G., Nasonov S.V., Novoselov M.M., Penner I.E., Samoilova S.V. "Investigations of the crystalline particle orientation in high-level clouds with a scanning lidar," ", Proc. SPIE 10833, 24th International Symposium on Atmospheric and Ocean Optics: Atmospheric Physics, 1083347 (13 December 2018); https://doi.org/10.1117/12.2504129

Konoshonkin, A.V., "Simulation of the scanning lidar signals for a cloud of monodisperse quasi-horizontal oriented particle," Optika Atmosfery i Okeana, 29, No. 12, 1053–1060 (2016) [in Russian].)

Konoshonkin, A., Wang, Zh., Borovoi, A., Kustova, N., Liu D., and Xie, Ch.: Backscatter by azimuthally oriented ice crystals of cirrus clouds, Opt. Express, 24(18), A1257-1268, 2016.

Lavigne, C., Roblin, A., and Chervet, P.: Solar glint from oriented crystals in cirrus clouds, Appl. Opt., 47(3), 6266–6276, 2008.

Liou, K. N.: Influence of cirrus clouds on weather and climate processes: a global perspective, J. Geophys. Res., 103, 1799–1805, 1986.

Madonna, F., Rosoldi, M., Lolli, S., Amato, F., Vande Hey, J., Dhillon, R., Zheng, Y., Brettle, M., and Pappalardo, G.: Intercomparison of aerosol measurements performed with multi-wavelength Raman lidars, automatic lidars and ceilometers in the framework of INTERACT-II campaign, Atmos. Meas. Tech., 11, 2459–2475, 2018.

Masuda, K. and Ishimoto, H.: Influence of particle orientation on retrieving cirrus cloud properties by use of total and polarized reflectances from satellite measurements, J. Quant. Spectrosc. Radiat. Transfer, 85, 183–193, 2004.

McCullough, E. M., Sica, R. J., Drummond, J. R., Nott, G., Perro, C., Thackray, C. P., Hopper, J., Doyle, J., Duck, T. J., and Walker, K. A., Depolarization calibration and measurements using the CANDAC Rayleigh–Mie–Raman lidar at Eureka, Canada, Atmos. Meas. Tech., 10, 4253–4277, 2017.

McCullough, E. M., Sica, R. J., Drummond, J. R., Nott, G. J., Perro, Ch., and Duck, T. J.: Three-channel single-wavelength lidar depolarization calibration, Atmos. Meas. Tech., 11, 861–879, 2018.

McGill, M. J., Hlavka, D. L., Hart, W. D., Spinhirne, J. D., Scott, V. S., and Schmid, B.: The Cloud Physics Lidar: Instrument description and initial measurement results, Appl. Opt., 41, 3725–3734, 2002.

Mishchenko, M. I. and Hovenier, J. W.: Depolarization of light backscattered by randomly oriented nonspherical particles, Opt. Lett., 20, 1356–1358, 1995.

Neely, R. R., Hayman, M., Stillwell, R. A., Thayer, J. P., Hardesty, R. M., O'Neill, M., Shupe, M. D., and Alvarez, C.: Polarization Lidar at Summit, Greenland for the Detection of Cloud Phase and Particle Orientation, J. Atmos. Ocean. Tech., 30, 1635–1655, 2013.

Noel, V. and Chepfer, H.: A global view of horizontally oriented crystals in ice clouds from Cloud-Aerosol Lidar and Infrared Pathfinder Satellite Observation (CALIPSO), J. Geophys. Res., 115, D00H23, 2010.

Noel, V. and Sassen, K.: Study of ice crystal orientation in ice clouds from scanning polarization lidar observations, J. Appl. Meteorol., 44(5), 653–664, 2005.

Noel, V., Chepfer, H., Ledanois, G., Delaval, A., and Flamant, P. H., Classification of particle effective shape ratios in cirrus clouds based on the lidar depolarization ratio, Appl. Opt., 41(21), 4245–4257, 2002.

Nott, G., Duck, T., Doyle, J., Coffin, M., Perro, C., Thackray, C., Drummond, J., Fogal, P., McCullough, E., and Sica, R.: A remotely operated lidar for aerosol, temperature, and water vapor profiling in the High Arctic, J. Atmos. Ocean. Tech., 29, 221–234, 2012.

Pal, S. R. and Carswell, A.I.: Polarization properties of lidar scattering from clouds at 347 nm and 694 nm, Appl. Opt., 17(15), 2321-2328, 1978.

Platt, C. M. R.: Lidar observations of a mixed-phase altostratus cloud, J. Appl. Meteorol., 16, 339–345, 1977.

Platt, C. M. R.: Lidar backscatter from horizontal ice crystal plates, J. Appl. Meteor., 17, 482–488, 1978.

Platt, C. M. R., Abshire, N. L., and McNice, G. T.: Some Microphysical Properties of an Ice Cloud from Lidar Observation of Horizontally Oriented Crystals, J. Appl. Meteorol., 17(8), 1220–1224, 1978.

Reichardt, J., Wandinger, U., Klein, V., Mattis, I., Hilber, B., and Begbie, R.: RAMSES: German Meteorological Service autonomous Raman lidar for water vapor, temperature, aerosol, and cloud measurements, Appl. Opt., 51(34), 8111-8131, 2012.

Samokhvalov, I.V., Nasonov, S.V., Stykon, A.P., Bryukhanov, I.D., Borovoi, A.G., Volkov, S.N., Kustova, N.V., and Konoshonkin, A. V., "Investigation of phase matrices of cirrus containing ensembles of oriented ice particles," Proc. SPIE 9292, 20th International Symposium on Atmospheric and Ocean Optics: Atmospheric Physics, 92922M (25 November 2014); doi: 10.1117/12.2075562

~~Summa, D., Di Girolamo, P., Stelitano, D., and Cacciani, M.: Characterization of the planetary boundary layer height and structure by Raman lidar: comparison of different approaches, Atmos. Meas. Tech., 6, 3515–3525, 2013.~~

~~Thomas, L., Cartwright, J. C., and Wareing, D. P.: Lidar observation of the horizontal orientation of ice crystals in cirrus clouds, Tellus 42B, 211–216, 1990.~~

Sassen, K.: Ice crystal habit discrimination with the optical backscatter depolarization technique, J. Appl. Meteor., 16, 425–431, 1977.

Sassen, K.: Corona-producing cirrus cloud properties derived from polarization lidar and photographic analyses, Appl. Opt., 30(24), 3421-3428, 1991.

Sassen, K. and Benson, S.: A midlatitude cirrus cloud climatology from the Facility for Atmospheric Remote Sensing: II. Microphysical properties derived from lidar depolarization, J. Atmos. Sci., 58(15), 2103–2112, 2001.

Sassen, K., Griffin, M. K., and Dodd, G. C.: Optical scattering and microphysical properties of subvisual cirrus clouds, and climatic implications, J. Appl. Meteorol., 28(2), 91-98, 1989.

She, C.-Y.: Spectral structure of laser light scattering revisited: Bandwidths of nonresonant scattering lidars, Appl. Opt., 40, 4875–4884, 2001.

Simonova, G. V., Balin, Yu. S., Kokhanenko, G. P., Ponomarev, Yu. N., and Rynkov, O. A., Scanning multi-wave lidar for atmosphere objects sensing~~sounding~~, Invention patent of Russian Federation, № 2593524, 2015.

Spinhirne, J. D., Hansen, M. Z., and Caudill, L. O. Cloud top remote sensing by airborne lidar, Appl. Opt., 21, 1564–1571, 1982.

Stillwell, R. A., Neely III, R. R., Thayer, J. P., Shupe, M. D., and Turner, D. D.: Improved cloud-phase determination of low-level liquid and mixed-phase clouds by enhanced polarimetric lidar, Atmos. Meas. Tech., 11, 835–859, 2018.

Strawbridge, K. B.: Developing a portable, autonomous aerosol backscatter lidar for network or remote operations, Atmos. Meas. Tech., 6, 801–816, 2013.

Summa, D., Di Girolamo, P., Stelitano, D., and Cacciani, M.: Characterization of the planetary boundary layer height and structure by Raman lidar: comparison of different approaches, Atmos. Meas. Tech., 6, 3515–3525, 2013.

Thomas, L., Cartwright, J. C., and Wareing, D. P.: Lidar observation of the horizontal orientation of ice crystals in cirrus clouds, Tellus 42B, 211–216, 1990.

Tao, Z., McCormick, M. P., Wu, D., Liu, Z., and Vaughan, M. A.: Measurements of cirrus cloud backscatter color ratio with a two-wavelength lidar, Appl. Opt., 47(10), 1478-1485, 2008.

Vaughan, M. A., Liu, Z., McGill, M. J., Hu, Y., and Obland, M. D., On the spectral dependence of backscatter from cirrus clouds: Assessing CALIOP's 1064 nm calibration assumptions using cloud physics lidar measurements, J. Geophys. Res., 115, D14206, 2010.

Veselovskii, I., Goloub, P., Podvin, T., Tanre, D., Ansmann, A., Korenskiy, M., Borovoi, A., Hu, Q., and Whiteman, D.N. Spectral dependence of backscattering coefficient of mixed phase clouds over West Africa measured with two-wavelength Raman polarization lidar: Features attributed to ice-crystals corner reflection, J. Quant. Spectrosc. Radiat. Transf., 202, 74–80, 2017.

Whiteman, D. N., Veselovskii, I., Cadirola, M., Rush, K., Comer, J., Potter, J., and Tola, R.: Demonstration Measurements of Water Vapor, Cirrus Clouds, and Carbon Dioxide Using a High-Performance Raman Lidar, J. Atmos. Ocean. Tech., 24, 1377–1388, 2007.

Volkov, S. N., Kaul, B. V., and Samokhvalov, I. V.: A technique for processing of lidar measurements of backscattering matrices, Atmos. Oceanic Opt., 15, 891–895, 2002.

Yoshida, R., Okamoto, H., Hagihara, Y., and Ishimoto, H.: Global analysis of cloud phase and ice crystal orientation from Cloud-Aerosol Lidar and Infrared Pathfinder Satellite Observation (CALIPSO) data using attenuated backscattering and depolarization ratio, J. Geophys. Res., 115, D00H3, 2010.

You, Y., Kattawar, G. W., Yang, P., Hu, Y. X., and Baum, B. A.: Sensitivity of depolarized lidar signals to cloud and aerosol particle properties, J. Quant. Spectrosc. Radiat. Transf., 100(1-3), 470–482, 2006.

Young, A. T.: Revised depolarization corrections for atmospheric extinction, Appl. Opt., 19, 3427–3428, 1980.

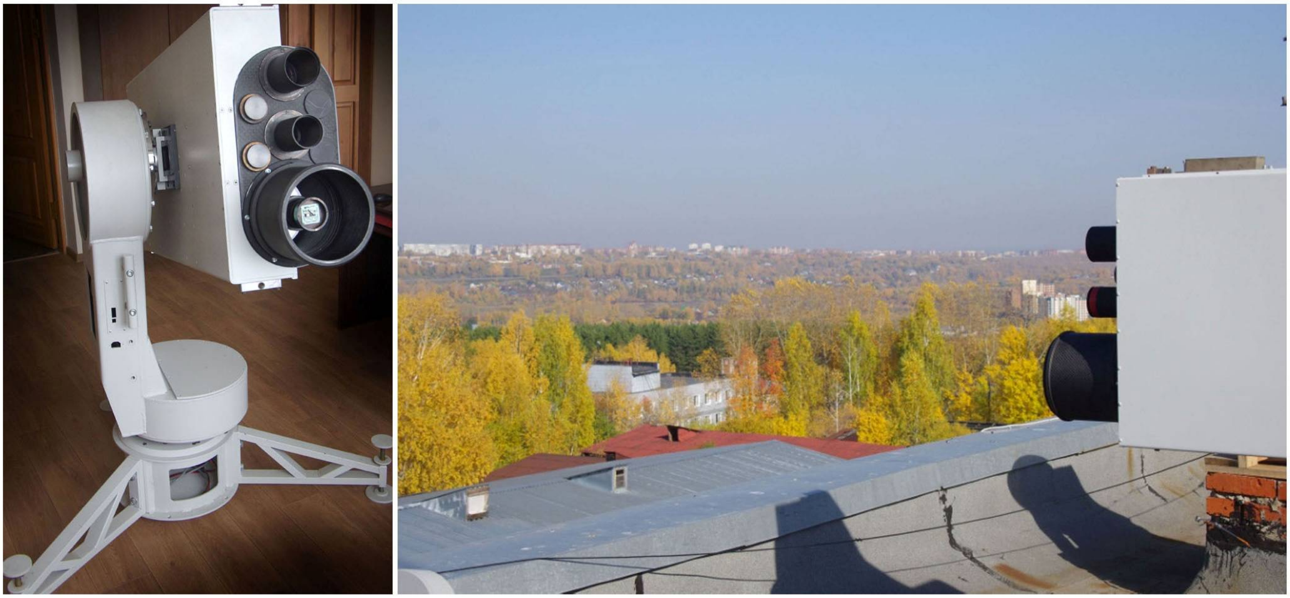

Figure 1. Photographs of the lidar on a rotary column in the laboratory room (left) and on the institute building roof (right).

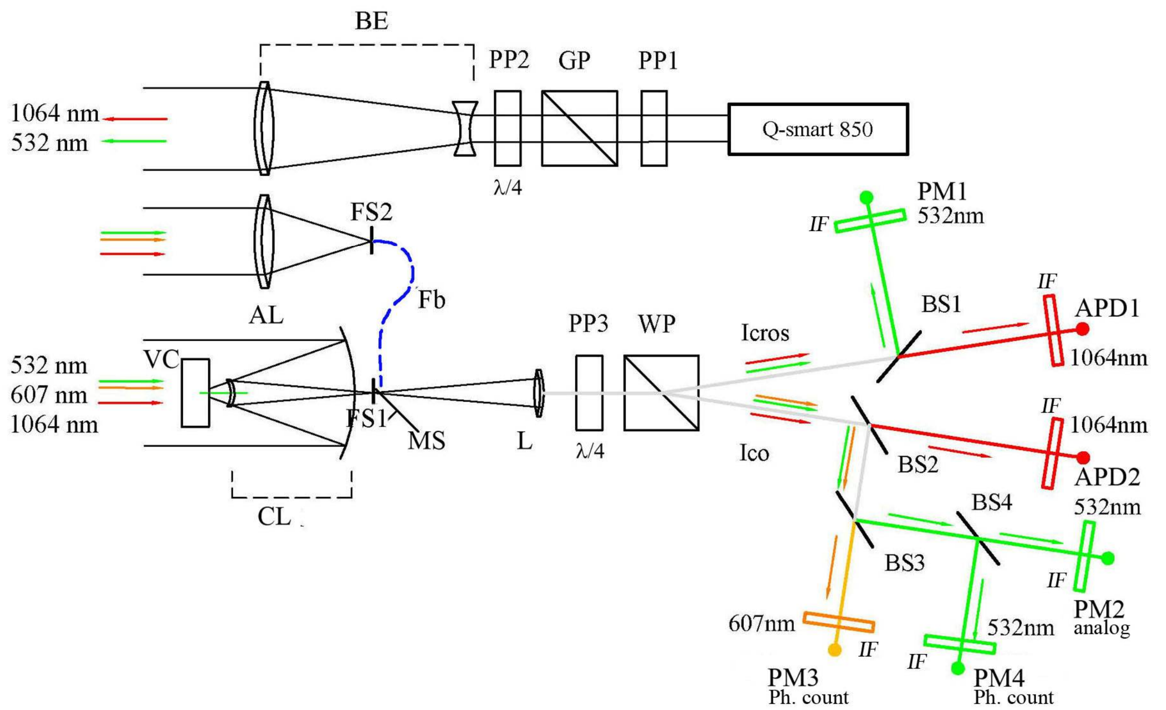

Figure 2. Optical circuit of the LOSA-M3 lidar. PP: phase plates; GP: Glan prism; BE: achromatic beam expander; AL: achromatic lens 40 mm diameter; CL: Cassegrain mirror lens *CL* 200 mm diameter; VC: video camera; FS1, FS2: iris diaphragms; Fb: optic fiber; MS: mirror shutter; L: lense; WP: Wollaston prism; BS: beamsplitters; APD: avalanche photodiodes; PMT: photomultiplier tubes.

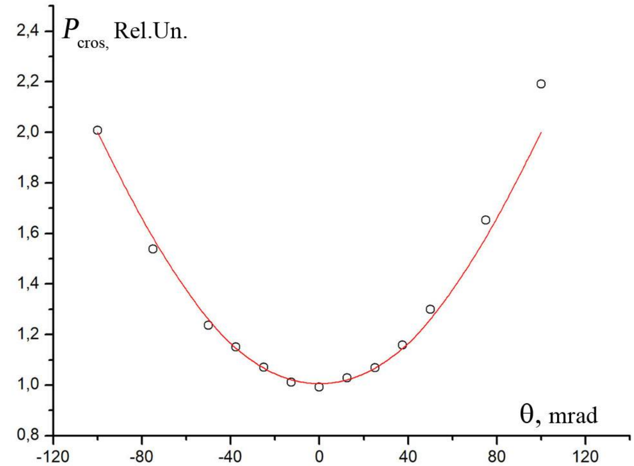

Figure 3. Adjusting the position of the Glan prism. The dependence of the cross-polarized component P_{cros} (normalized to the minimum = 1) on the angle θ of the prism rotation is shown. Measured values P_{cros} (circles) and fitting curve (red line).

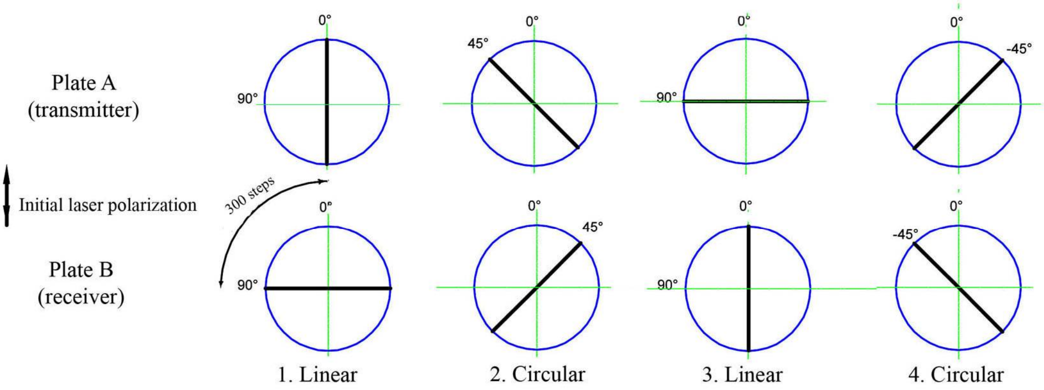

Figure 4. Diagram of the rotation of the phase plates. Plate mounting angles for the four consecutive laser pulses are shown. The bold line shows the direction of a fast axis of the plates.

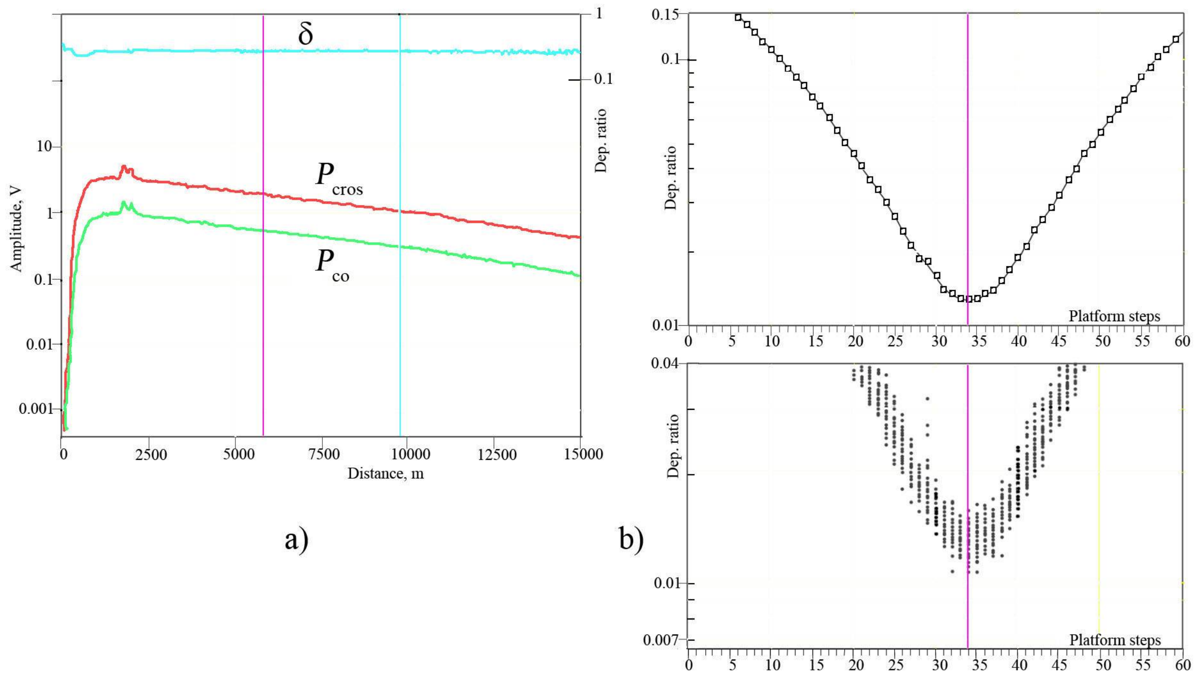

Figure 5. (a) Lidar signals from two photodetectors (P_{co} and P_{cros}), summarized over all positions of plate B (red and green lines). A height range 6-9 km with constant depolarization ratio (blue line) is chosen to adjust the plates. (b) Depolarization ratio for each pulse (bottom) and averaged over a 30 minute record (top).

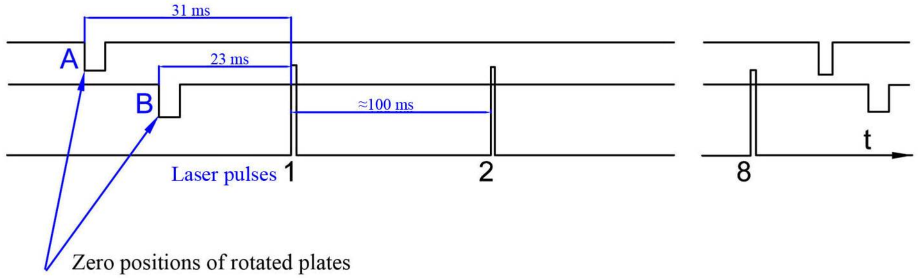

Figure 6. Time positions of the laser pulses relative to the zero positions of the plates. The situation repeats every 8 pulses.

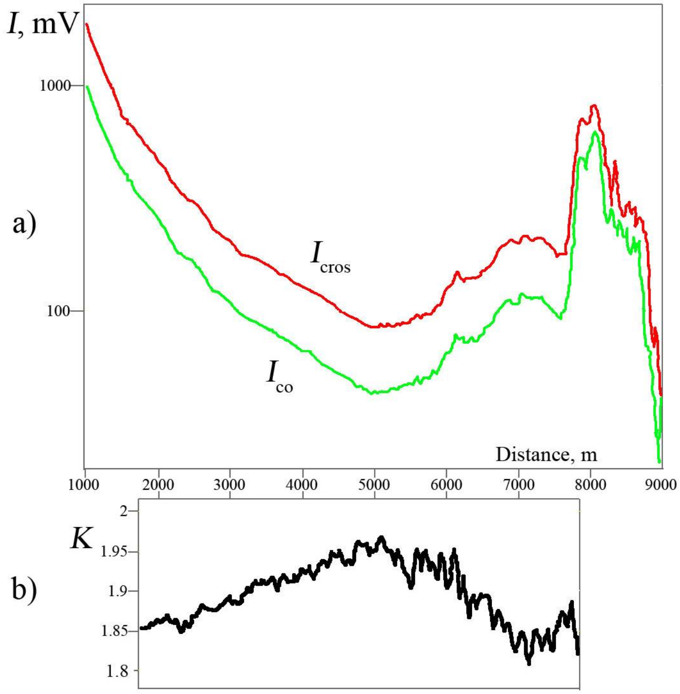

Figure 7. Channel calibration procedure. (a) The record of a signal (1064 nm) integrated by the plate rotation angle, components I_{co} (green) and I_{cros} (red). Integration was carried out during four revolutions of the plate. (b) the value of calibration constant *K*, calculated in the height range of 1800-8000 m. The mean value *K*=1.91.

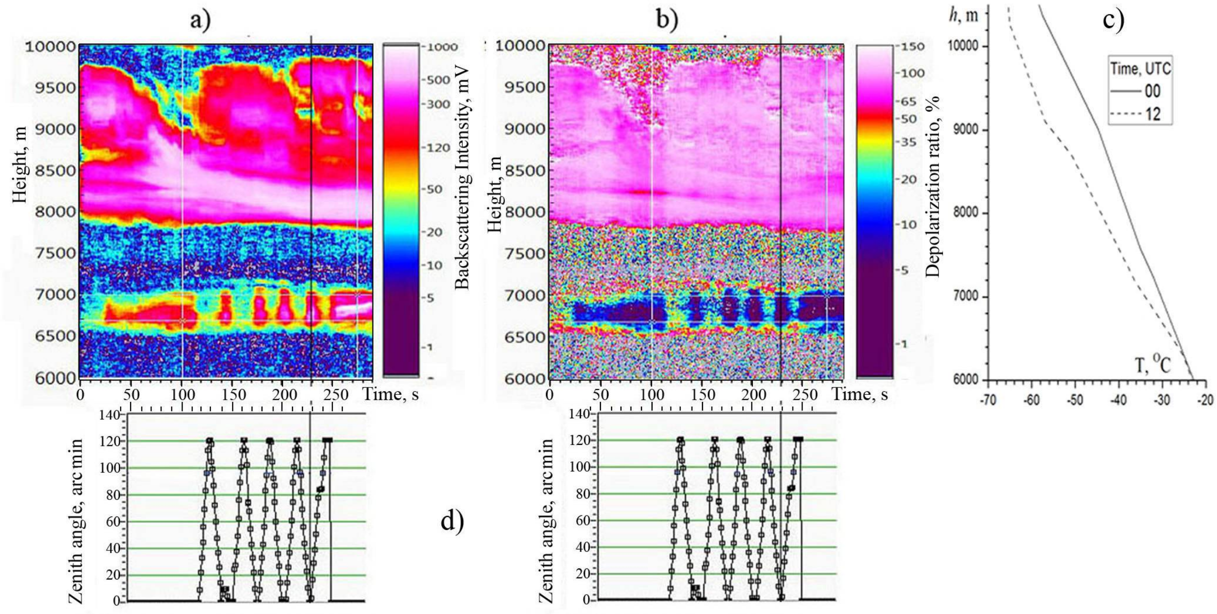

Figure 8. Lidar data on 6 April 2018, 10:25 LST (UTC+7) for the initial circular polarization. (a) Intensity of I_{co}^{Circ} component; (b) depolarization ratio $\delta^{Circ} = I_{cros}^{Circ} / I_{co}^{Circ}$; (c) weather sounding data (Novosibirsk station, 07:00 and 19:00 LST); (d) zenith tilt angle (arc min), time axis is aligned with 7a and 7b.

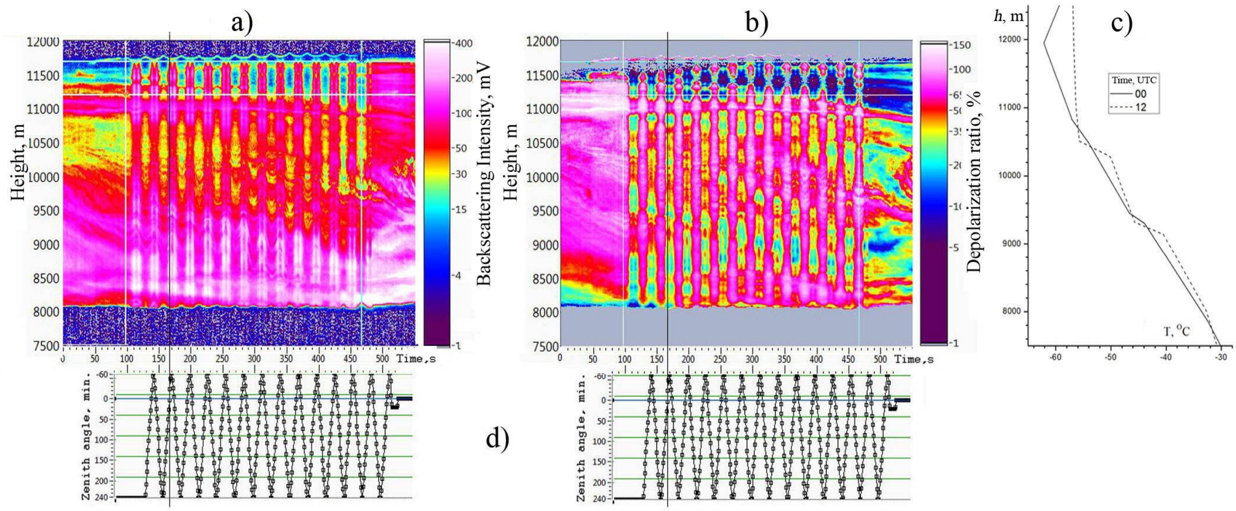

Figure 9. Lidar data on 2 June 2018, 09:55 LST. Designations as in Fig. 7.

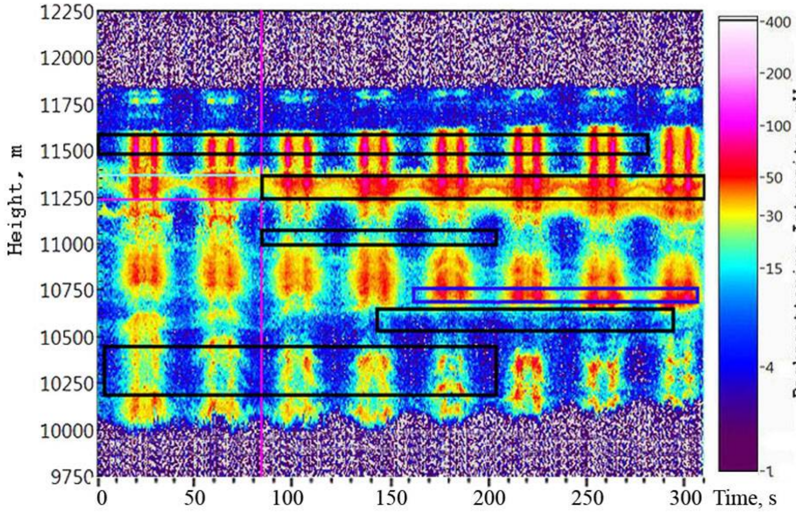

Figure 10. Selection of cloud sections for further processing. Recorded on 2 June 2018, 12:00-12:05 LST. Rectangles highlight areas which have a pronounced dependence on the tilt angle, and there is no signal overflow when the lidar is oriented to zenith.

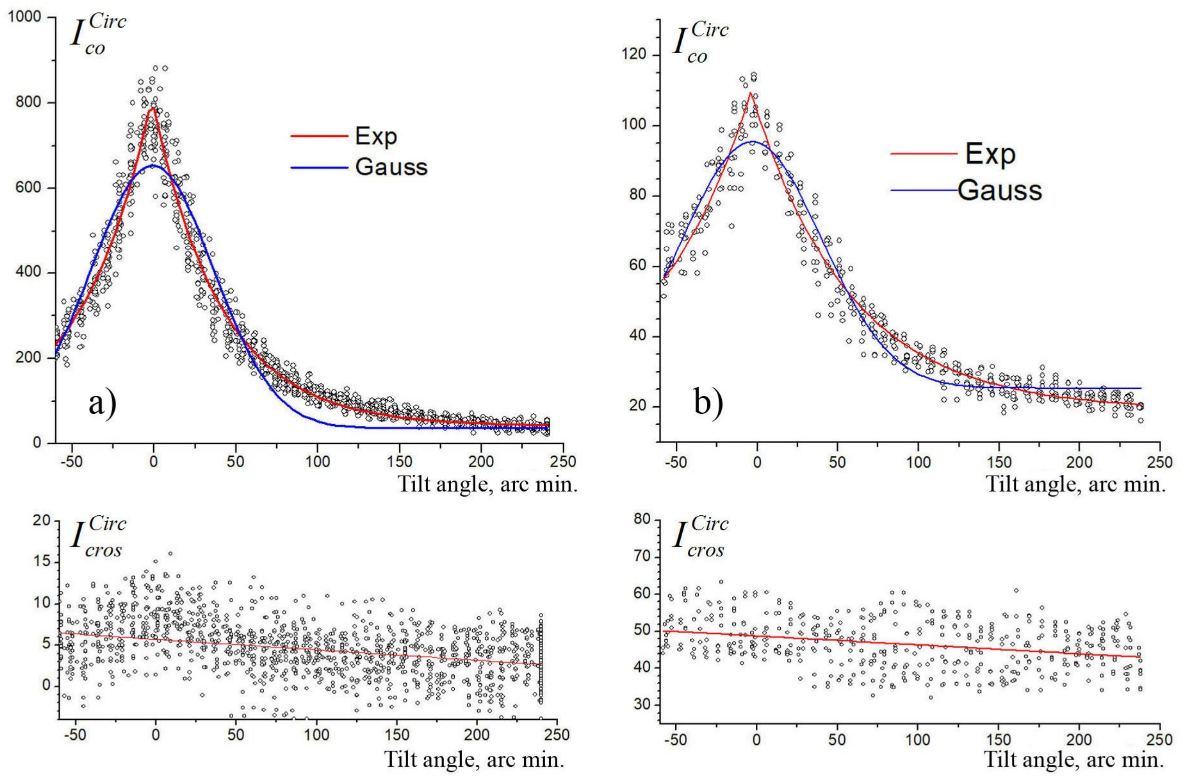

Figure 11. Typical angular dependences of the intensity of polarization components, 2 June 2018. Top frames – co-polarized components I_{co}^{Circ}, bottom frames - I_{cros}^{Circ}. (a) 12:00 LST, averaging over the layer from 11470m to 11600m. (b) 10:00 LST, the layer 10980-11270 m. The record (a) shows low depolarization ratio and narrow (*w*=42 arc min.) distribution. The record (b) has a wider distribution (*w*=82 arc min.) and large depolarization

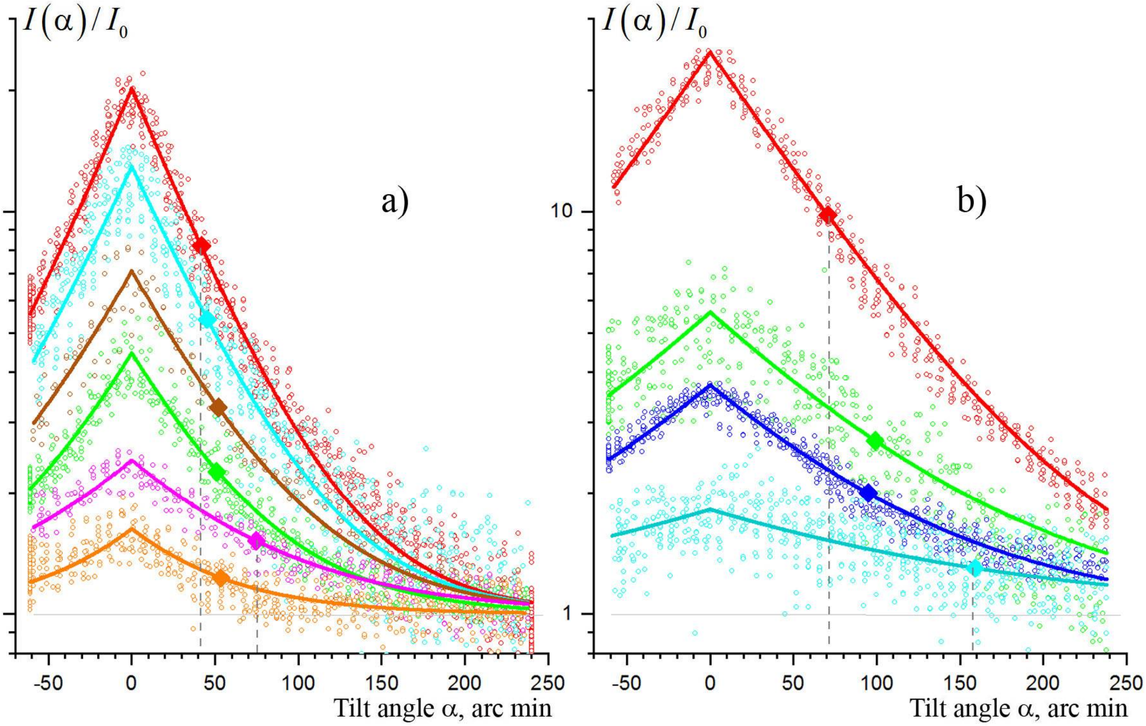

Figure 12. Selected cases of observed distributions I_{co}^{Circ}. For all curves the values of intensity are normalized to the values I_0. obtained by fitting according to the Eq. (1). Squares indicate the tilt angles, corresponding to the distribution width *w*. The left frame shows cases of a fairly narrow distribution, *w* is within 40-75 arc minutes. The ratio $I(4°)/I_0$ is less then 1.1. The right frame shows cases with $I(4°)/I_0 > 1.1$, among these cases there are distributions with a large (up to 159 arc min) width.

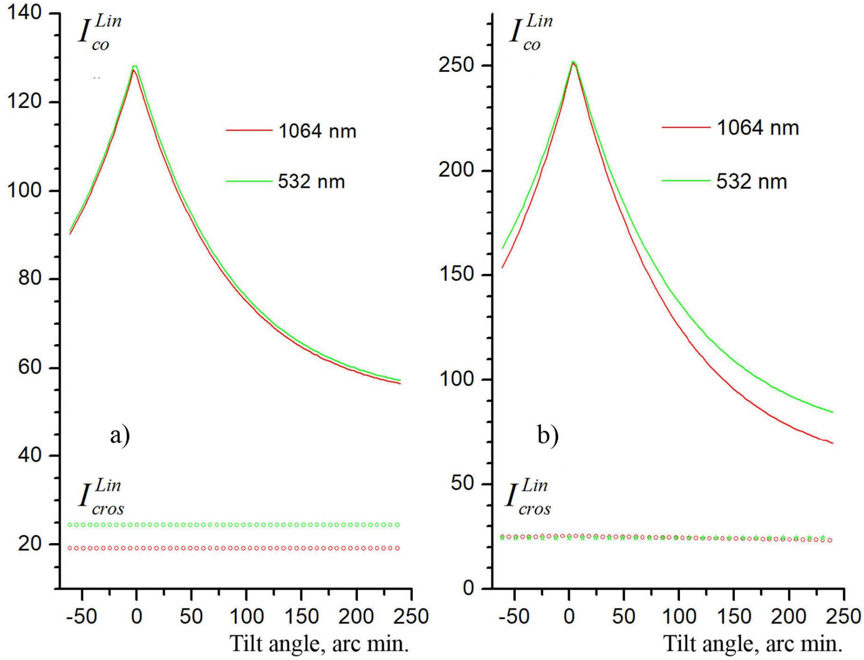

Figure 13. Angular dependencies of polarization components for 532 nm (green) and 1064 nm (red). Two cases with the maximum angular differences are shown. In all other cases the distribution width *w* for 532 nm is equal or bigger than for 1064 nm.